

1 **Diatom–environment relationships and limnological variability: an**
2 **updated quantitative tool for palaeoclimatological studies on sub-**
3 **Antarctic Macquarie Island**

4 Caitlin A. Selfe¹, Karina Meredith², Liza McDonough², Justine Shaw¹, Stephen J. Roberts³, Krystyna M.
5 Saunders^{4,5}

6

7 ¹ Securing Antarctica’s Environmental Future, Queensland University of Technology, Brisbane, 4000,
8 Australia

9 ² Securing Antarctica’s Environmental Future, Environment Research and Technology Group, Australian
10 Nuclear Science and Technology Organisation, Lucas Heights, 2234, Australia

11 ³ British Antarctic Survey, Cambridge, CB3 0ET, United Kingdom

12 ⁴ Institute for Marine and Antarctic Studies, University of Tasmania, Hobart, 7004, Australia

13 ⁵ Australian Antarctic Division, Kingston, 7050, Australia

14

15 *Correspondence to:* Caitlin A. Selfe (caitlin.selfe@hrd.qut.edu.au)

16 **Keywords:** Diatoms, Electrical conductivity, sub-Antarctic, Macquarie Island, Transfer function, Southern

17 Hemisphere westerly winds, Palaeoclimate, Limnology

18 **Abstract.** Sub-Antarctic Macquarie Island is ideally located for reconstructing past variations in Southern
19 Hemisphere westerly wind strength. Diatoms are a valuable palaeolimnological tool on sub-Antarctic
20 islands, providing a means to reconstruct past climate and environmental changes. Diatom communities
21 are sensitive to changes in lake electrical conductivity (EC) linked to westerly wind-driven sea-spray
22 inputs on Macquarie Island, and diatom-conductivity models have previously been used to infer past
23 westerly wind variability. Here we present new diatom data from 52 lakes to assess diatom-environment
24 relationships and develop an updated diatom-conductivity model for Macquarie Island. Seasonal and
25 multi-year water chemistry and isotope data were analysed to assess temporal variability in
26 hydrochemical processes and the influence of evaporation, ensuring the resulting diatom-conductivity
27 model reflects external climatic drivers rather than local dynamics. Statistically robust transfer functions
28 were developed for EC (bootstrapped $r^2 = 0.80$, RMSEP = 0.40), while pH and temperature had weaker
29 predictive performance. For EC, weighted averaging and maximum-likelihood approaches performed
30 comparably, although the former showed reduced predictive power at high EC where low species
31 turnover and nutrient collinearity affected accuracy. This quantitative-diatom model combined with
32 understanding of hydrogeochemical processes provides an improved basis for reconstructing past
33 Southern Hemisphere westerly wind variability, which can be applied in future palaeoclimate studies on
34 Macquarie Island.

35

36

37 **1 Introduction**

38 The Southern Ocean region exerts a strong influence on Southern Hemisphere and global climates
39 (Jones et al. 2016; Fogt and Marshall 2020). Sub-Antarctic islands are among the few landmasses
40 located in the Southern Ocean, making them important sites for understanding the past and future role
41 of the Southern Ocean on climate variability. The Southern Hemisphere westerly winds (SHW) are a
42 major driver of Southern Hemisphere mid- to high-latitude climates, modulating ocean circulation, mid-
43 latitude temperature and precipitation regimes, and the efficiency of the Southern Ocean carbon sink
44 (Gillett et al. 2006; Le Quéré et al. 2009; Fletcher et al. 2021; Menviel et al. 2023; Thomas et al. 2025).
45 Instrumental data show that in recent decades the SHW have intensified and shifted poleward in
46 response to warming (Marshall 2003; Fogt and Marshall 2020). These changes have been linked to an
47 increase in net outgassing of carbon dioxide (CO₂) from deep-storage reservoirs in the Southern Ocean,
48 with significant implications for future atmospheric CO₂ levels and global temperatures (Goyal et al. 2021;
49 Nicholson et al. 2022; Mongwe et al. 2024; Olivier and Haumann 2025). Understanding long-term SHW
50 variability is key to assessing the impacts of SHW dynamics under future climate warming scenarios.

51

52 Diatoms are highly sensitive to environmental changes and are widely used as palaeolimnological
53 proxies to infer climate and environmental changes (Roberts et al. 2000; Verleyen et al. 2004; Sterken
54 et al. 2008; Recasens et al. 2015; Liao et al. 2020; Peng et al. 2022; Deng et al. 2025). Diatoms are well
55 established as indicators of salinity and ionic composition, forming the basis of numerous diatom–salinity
56 or -conductivity transfer functions across a range of environments (Gasse et al. 1997; Verleyen et al.
57 2003; Volik et al. 2017; Maslennikova 2020; Farqan et al. 2025). These approaches have been
58 successfully applied in diverse settings demonstrating the reliability of diatom assemblages for
59 reconstructing past hydrochemical and environmental change.

60

61 Previous work on sub-Antarctic Islands has demonstrated that aquatic diatom communities are
62 significantly influenced by changes in salinity (inferred from electrical conductivity, EC), allowing
63 quantitative diatom-conductivity models to be developed (Gremmen et al. 2007; Saunders et al. 2009;
64 2015; 2018; Perren et al. 2020; Van Nieuwenhuyze 2020; Perren et al. 2025). On sub-Antarctic islands,
65 lake water salinity changes are largely controlled by wind-driven sea spray aerosol (SSA) inputs, via both
66 wet and dry deposition, with increased inputs occurring when winds are stronger and vice versa (Evans

67 1970; Buckney and Tyler 1974; Saunders et al. 2009; 2015; Humphries et al. 2021). Based on this,
68 diatom-conductivity transfer functions have been used to infer past Holocene SHW intensity on
69 Macquarie Island (Saunders et al., 2018), Marion Island (Perren et al. 2020) and in southern South
70 America (Perren et al. 2025). These relationships are understood to reflect longer-term, integrated
71 hydrogeochemical and ecological responses to persistent wind-driven sea-spray inputs, rather than
72 event-scale meteorological forcing.

73

74 Earlier studies on Macquarie Island have analysed diatom-environment relationships (McBride 2009;
75 Saunders et al. 2009) and their application as palaeoenvironmental and climate proxies (Keenan 1995;
76 Saunders et al. 2013; 2018; Deng et al. 2025). However, from the late 1900s to early 2000s overgrazing
77 from increasing invasive rabbit populations (up to 150,000 individuals estimated from 2005-2006)
78 resulted in widespread ecosystem degradation, including erosion, vegetation loss, and altered organic
79 inputs into lakes (Scott and Kirkpatrick 2008; Terauds 2009). This affected aquatic ecosystems and
80 diatom diversity (Marchant et al. 2011; Saunders et al. 2013). The Macquarie Island Pest Eradication
81 Programme successfully eradicated all invasive vertebrates (principally rabbits) from the island in 2011,
82 triggering substantial ecosystem recovery (Springer, 2018; Fitzgerald et al., 2021). Although direct
83 limnological data to assess ecosystem recovery of individual lakes is not available, widespread
84 vegetation recovery following early efforts of the eradication programme in 2010-2011 provides strong
85 evidence that ecosystem processes across the island are no longer characterised by extreme
86 disturbance (Shaw et al. 2011; Springer 2018; Fitzgerald et al. 2021). This is expected to have decreased
87 catchment erosion and sediment and nutrient delivery into lakes relative to the peak disturbance period,
88 resulting in post-eradication (recovering) ecosystems.

89

90 Reassessing diatom–environment relationships under current post-eradication conditions is necessary,
91 because earlier studies were conducted during a period of vertebrate-induced disturbance rather than
92 under near-natural conditions (Saunders et al., 2013). Developing new diatom models based on post-
93 eradication conditions may better represent pre-invasion baseline communities, improving the accuracy
94 and ecological relevance of palaeolimnological reconstructions. Furthermore, incorporating revised
95 taxonomy and newly identified species will enhance the model’s ecological resolution and predictive
96 performance.

97

98 Understanding the processes that drive lake water chemistry, such as precipitation, evaporation,
99 groundwater inputs, and nutrient cycling, and how they vary across temporal and spatial scales is
100 essential when interpreting diatom–environmental relationships. Meredith et al. (2022) defined
101 hydrogeochemical lake processes across Macquarie Island showing that dominant processes vary
102 locally, and lakes can be classified as predominantly influenced by SSAs, catchment processes (i.e.,
103 with greater water-rock interaction), or precipitation (i.e., more dilute lake waters). Sea-spray-influenced
104 lakes occur near the west coast and on the western edge on the Macquarie Island plateau, where
105 exposure to the SHW is greatest. In contrast, catchment-influenced lakes with higher terrestrial ion
106 concentrations are found at lower elevations, and rainfall-influenced lakes with low ion concentrations
107 occur at higher elevations. This hydrogeochemical framework supports the hypothesis that for lakes near
108 the west coast, including those on the western edge of the plateau, EC-related diatom variation on
109 Macquarie Island primarily reflects SHW-driven sea-spray inputs rather than local hydrological or
110 geochemical controls.

111

112 While present day water chemistry provides valuable insight into spatial variability, it is necessary to
113 quantify temporal variability in hydrogeochemical processes, particularly evaporation, to assess how
114 seasonal, interannual, and longer-term changes modify ion concentrations in lakes, including those
115 derived from SSA. Establishing seasonal and multi-year lake water hydrogeochemical datasets will
116 enhance confidence in proxy interpretations and form a foundation for long-term monitoring of Macquarie
117 Island lakes. Such research is rarely applied to develop ecological transfer functions particularly in such
118 remote, isolated settings, and has not yet been undertaken on other sub-Antarctic islands. These factors
119 highlight the importance of this work for understanding how sub-Antarctic Island ecosystems will respond
120 to future climate and environmental changes, particularly given the rapid ecological shifts in response to
121 climate that are already documented across the region (le Roux and McGeoch 2008; Lee and Chown
122 2016; Nel et al. 2023).

123

124 Here, we present new data from lakes on Macquarie Island quantifying post-pest eradication
125 relationships between surface-sediment diatom communities and environmental conditions. Using
126 comprehensive water chemistry datasets from 2018 and 2022–23, we examine seasonal and interannual
127 variability to develop updated diatom–environment transfer functions. This integrated approach
128 strengthens the application of diatom-based proxies and provides a first step towards long-term

129 monitoring of sub-Antarctic lake systems by contributing to baseline data and establishing an analytical
130 framework to track ecological and biogeochemical change. These transfer functions will be applied in
131 future studies to reconstruct past Holocene climate variability on Macquarie Island.

132 **2 Methods and Materials**

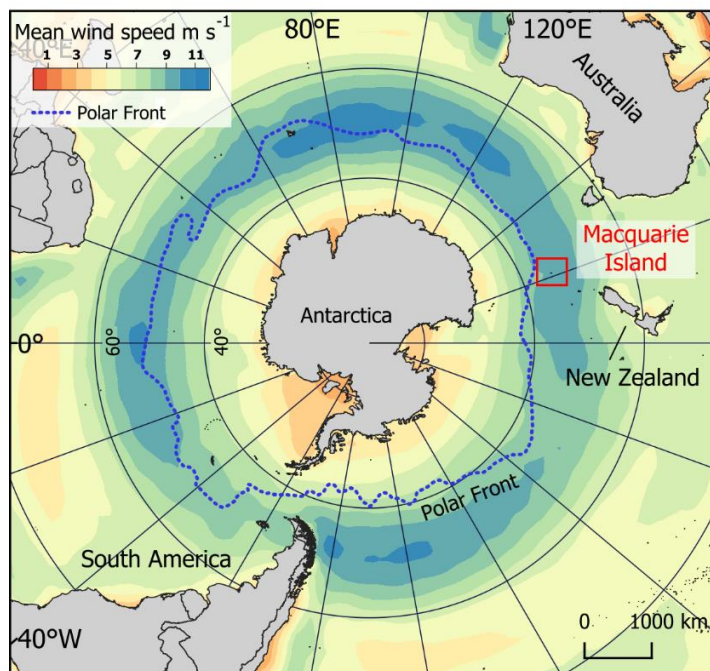
133 **2.1 Study area: Macquarie Island**

134 Macquarie Island (54°50'S, 158°85'E) is a small sub-Antarctic island (128 km²) located in the Southern
135 Ocean just north of the polar front, 1200 km south-west of New Zealand and 1300 km from the Antarctic
136 continent (Fig. 1). It is one of the few landmasses within the Polar Frontal Zone and modern core SHW
137 belt (50–55°S; Fig.1), making it ideally suited to study past and current changes in the SHW, temperature,
138 and precipitation. It has a harsh, cool, wet, oceanic climate with low seasonality and high wind velocities
139 throughout the year. Together, these represent the influence the SHW have on climate in the region
140 (Selkirk et al. 1990). The SHW prevail almost exclusively from the west and north-west with a mean
141 annual wind speed of 35 km h⁻¹ and gusts reaching 185 km h⁻¹ (between 1948-2025; BOM 2025). The
142 continual dominance of the SHW drive environmental and ecosystems responses on a west-to-east
143 gradient across the island (Chau et al. 2019; Meredith et al. 2022), including the deposition and
144 accumulation of wind-blown inputs such as sea spray and minerogenic aerosols (Buckney and Tyler
145 1974; Saunders et al. 2009). Mean annual temperature ranges from 3.1–6.6°C, and the island
146 experiences high annual rainfall of >1000 mm with >317 rainy days yr⁻¹ (between 1948–2025; BOM
147 2025). Rainfall has increased in recent decades with a higher frequency of intense rainfall events, mostly
148 occurring during winter, which are then accompanied by drier, windier summers (Andersen et al. 2009;
149 Kong et al. 2025). Persistent cloud cover over the island results in low light levels and sunshine hours
150 per day (average 2.4 h from 1948–2022; BOM, 2025).

151

152 Macquarie Island is geologically unique, being the only location worldwide where an intact marine
153 ophiolite sequence of oceanic crust and upper mantle is exposed above sea level (Davis, 1987). The
154 island is composed mostly of pillow basalts with interspersed flows of massive basalt (Selkirk et al. 1990).
155 Dolerite, ultrabasics and intrusives are also present but are confined to the northern third of the island
156 (Mawson 1943). As widespread glaciation did not occur during the Last Glacial Maximum (26–20 ka),
157 marine, periglacial and subaerial erosional, rather than glacial processes, shaped the island as well as

158 lake formation and ontogeny. The island is fringed by a low coastal terrace leading to steep-sided slopes
159 (20–40°) that rise to form the island plateau sitting at ~200–400 m asl (Selkirk et al. 1990; McBride and
160 Selkirk 1998).



161
162 Fig 1: Location of Macquarie Island in the Southern Ocean and mean annual wind speeds around the Southern Hemisphere
163 (ERA5 reanalysis data 1960-2025), showing that the island lies within the modern core Southern Hemisphere westerly wind
164 belt (50–55°S).

165 The island has numerous shallow and deep lakes and ponds across the plateau and coastal terrace (Fig.
166 2). High accumulation of surface water and a high water-table at or very near the surface lead to the
167 formation of extensive mires across the island (Löffler 1984). While lake edges can form thick ice cover
168 during winter, complete freezing of the lakes is not typically observed (Evans 1970; Selkirk-Bell and
169 Selkirk 2013). The island is vegetated by bryophytes, tussock grass, herbs and sedges, with no shrub
170 or tree species present (Selkirk et al. 1990).

171 2.2 Data collection

172 Surface sediments and water samples were collected from lakes on Macquarie Island during the 2022–
173 23 austral summer (referred to as 2022). Sites were selected to replicate those sampled in 2018 that
174 were published by Meredith et al. (2022).

175 Lake surface sediments were collected from 30 plateau (inland) sites for diatom analyses (lake ID = LK),
176 representing conditions more than 10 years post-rabbit and rodent eradication. Surface sediments (top
177 2 cm) were collected from each site using a long-handled scoop from <1.5 m water depth. This method
178 for sediment collection was selected for its logistical feasibility. Sediment mixing was minimised by
179 visually assessing sampling depth and subsampling where necessary to retain only the upper ~2 cm.
180 Sediments were generally well consolidated and remained intact during collection. Based on available
181 lead-210 (^{210}Pb) chronologies from Macquarie Island lake cores, this interval represents approximately
182 10 years of accumulation (Saunders et al. 2013; Saunders et al. 2018), comparable to surface sediment
183 sampling approaches used in previous studies (e.g. Saunders et al., 2009). An additional 17 coastal and
184 five plateau sites sampled in 2006 (lake ID = S; Saunders et al. 2009) were included in the diatom dataset
185 to extend the EC and nutrient gradients of the updated dataset, totalling 52 samples (Fig. 2a). Two lakes
186 were replicated in the 2006 and 2022 seasons (S9 = LK40, S18 = LK2; Fig. 2a).

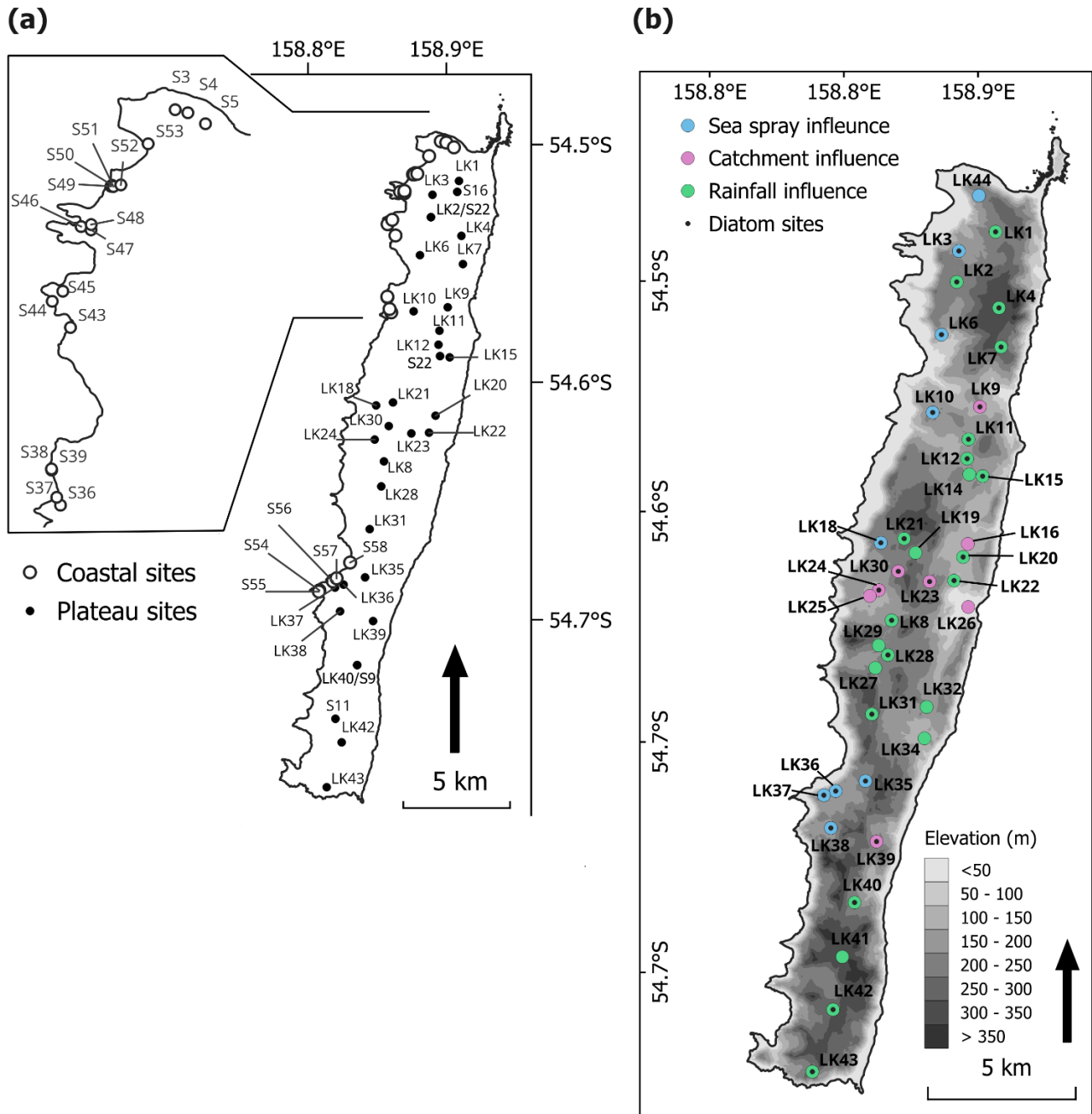
187

188 Lake water general parameters were measured in-situ at each site, including temperature, EC, dissolved
189 oxygen (DO), and pH using a YSI ProQuatro Multiparameter Meter, with calibration performed prior to
190 every sampling trip. DO was calibrated in water-saturated air following YSI manufacturer protocols.
191 Conductivity was calibrated using a $1413 \mu\text{S cm}^{-1}$ standard solution, and pH was calibrated using a
192 three-point procedure with pH 4.0, 7.0, and 10.0 buffer solutions. Water samples were collected at all
193 diatom sampling sites to measure total oxidised nitrogen (TON), phosphate (PO_4^{3-}), and silica (Si).
194 Additional water samples were collected from 40 plateau sites for water chemistry analysis (Fig. 2b),
195 including major ions and stable water isotopes (oxygen [$\delta^{18}\text{O}$] and hydrogen [$\delta^2\text{H}$]). Each site was
196 sampled three times across the 2022–23 season (November, December to January, and February). All
197 water samples were collected from ~20 cm below the water surface and were filtered in-situ with 0.45
198 μm polyethersulphone filters into High Density Poly-Ethylene (HDPE) bottles following the method
199 described by Meredith et al. (2009)). Water samples were refrigerated (4°C) until analysis.

200

201 Major ions, and oxygen ($\delta^{18}\text{O}$) and hydrogen ($\delta^2\text{H}$) stable isotopes were analysed at the Australian
202 Nuclear Science and Technology Organisation (ANSTO). Cations and anions were analysed using
203 inductively coupled plasma-atomic emission spectrometry (ICP-AES). $\delta^{18}\text{O}$ and $\delta^2\text{H}$ stable isotopes were
204 analysed with a Picarro L2130-i Cavity Ring-Down Spectrometer. Values were reported as per mill (‰)

205 deviations relative to the international standard V-SMOW (Vienna Standard Mean Ocean Water), with a
206 reproducible precision of ± 0.2 and $\pm 1.0\text{‰}$, respectively.



207 Fig. 2: Maps showing lake sites across Macquarie Island, **a**) Diatom surface sediment sites (coastal sites were originally sampled
208 by Saunders et al. (2009); **b**) Lake water chemistry sites. Colours show lake types, based on dominate hydrogeochemical
209 processes, identified by Meredith et al., (2022). Black dots indicate that the site is also included in the diatom dataset.

210 Nutrient data from 2006 samples (filtered at 0.45 μ m) measured soluble reactive phosphate (SRP), TON
211 (nitrate [NO₃] + nitrite [NO₂]), and silicate (Si) using an Alpkem Autoanalyser (Continuous Flow Solution
212 Analyser), representing the operationally defined dissolved inorganic (and therefore readily bioavailable)
213 fractions of total N, P, and Si. In contrast, the 2022 dataset measured TON, PO₄³⁻, and Si ions using
214 ICP-AES at ANSTO on filtered, undigested waters, with results reported as the corresponding inorganic
215 species and concentrations consistently at or near detection limits. Despite methodological differences,
216 the two approaches yield consistently low and broadly comparable concentrations in the two replicate
217 lakes across sampling trips: for S9/LK40, PO₄³⁻ concentrations were 0.002 mg L⁻¹ (autoanalyser) and
218 <0.01 mg L⁻¹ (ICP-AES), and TON concentrations were 0.006 mg L⁻¹ (autoanalyser) and <0.06 mg L⁻¹
219 (ICP-AES); for S18/LK2, PO₄³⁻ concentrations were 0.004 mg L⁻¹ (autoanalyser) and <0.01 mg L⁻¹ (ICP-
220 AES), and TON concentrations were 0.005 mg L⁻¹ (autoanalyser) and < 0.06 mg L⁻¹ (ICP-AES).
221 Furthermore, if the 2022 analyses targeted the same reactive fractions measured in 2006, the results
222 would still fall below or close to detection limits.

223 **2.3 Diatom preparation and identification**

224 Diatom preparation followed methods described by McBride (2009). Cleaned diatom solutions were
225 mounted onto slides using Norland Optical Adhesive 61. At least 300–400 frustules were counted per
226 sample, using Differential Interference Contrast (DIC) and oil immersion at 1000x magnification on a
227 Zeiss Axioskope microscope, mounted with a TOUPTEK camera (U3CMOS). Species identification was
228 primarily based on sub-Antarctic taxonomy described in Van de Vijer et al. (2002); Sterken et al. (2015);
229 Sabbe et al. (2019); and Van de Vijver (2019). Species were photographed and documented (see
230 Supplementary Material for an illustrated species catalogue).

231 **2.4 Statistical analyses**

232 **2.4.1 Water chemistry**

233 The lake water chemistry dataset was comprised of *in-situ* general parameters, major ion concentrations
234 and $\delta^{18}\text{O}$ and $\delta^2\text{H}$ values from 2018 (Meredith et al. 2022) and 2022 (this study) to understand temporal
235 variation across the island. Data from 2018 (January to February) are referred to as sampling event 1
236 (E1) and sampling from the 2022 season as E2 (November), E3 (December to January), and E4
237 (February). Shapiro–Wilk tests showed that isotope data were normally distributed ($p > 0.05$), whereas

238 general parameters and ion concentrations deviated significantly from normality ($p < 0.05$).
239 Consequently, parametric tests (ANOVA, t-test, Tukey's HSD) were applied to normally distributed
240 isotope data, and non-parametric tests (Kruskal–Wallis, pairwise Wilcoxon) to non-normally distributed
241 general parameters ion data. A Principal Component Analysis (PCA) with z-score standardised data was
242 performed to explore relationships between variables and assess the consistency of lake types identified
243 by Meredith et al. (2022; Fig. 2b).

244 **2.4.2 Diatom model**

245 Diatom inference models were developed using diatom and environmental data collected from 2006 and
246 2022. Ordination methods were used to describe variation in the diatom dataset, explore diatom-
247 environment relationships, and identify unique variance explained by environmental variables.
248 Environmental variables included were EC, temperature, DO, pH, TON, PO_4^{3-} , and Si, with mean 2022
249 values used. Additional major ions were not included as these data were not available for 2006 sites.
250 Water depth was not included as a variable as all sediment samples were collected within a narrow range
251 of 0–1.5 m water depth, rendering ecological changes in depth negligible. Additionally, water depth is
252 often regarded as a composite variable that acts as a surrogate for complex environmental gradients
253 (e.g., habitat type, light, salinity, nutrients, oxygen, and taphonomy) that are largely unknown and
254 unquantified, and therefore its inclusion can lead to spurious and misleading results (Birks et al. 1998;
255 Juggins 2013). Weighted Averaging (WA) was applied to determine species ecological optima and
256 tolerance. Together WA, Weighted Averaging Partial Least Squares (WAPLS), and Maximum Likelihood
257 (ML) models were used to develop diatom transfer functions, with cross-validation used to assess model
258 robustness.

259

260 The relative abundance of each diatom species in each sample was calculated as the percentage of the
261 total number of frustules counted per sample. Species occurring at $\leq 1\%$ relative abundance were
262 excluded from the dataset. A full species list can be found in Supplementary Material. Nutrient values
263 that were below the limit of detection were substituted with the respective detection limit value (PO_4^{3-} , =
264 0.01 mg L^{-1} , Si = 0.1 mg L^{-1} , TON = 0.06 mg L^{-1}). Environmental variables were screened for skewness,
265 with temperature, EC, PO_4^{3-} , Si, and TON $\log(x+1)$ transformed.

266

267 PCA was performed on transformed environmental data to identify the primary gradients of
268 environmental variation across sites. Detrended Correspondence Analysis (DCA) with detrending by
269 segments and downweighting of rare species was performed on untransformed species data to
270 determine whether species distributions were linear or unimodal. As the DCA axis 1 gradient length (8.2
271 deviation units) was > 4 , unimodal ordination methods were deemed appropriate (Ter Braak and Prentice
272 1988). Species data were $\log(x+1)$ transformed for remaining analysis.

273

274 A series of Canonical Correspondence Analyses (CCA) were then performed with forward selection, and
275 scaling focused on inter-species distances, biplot scaling and downweighting of rare species. Variance
276 Inflation Factors (VIF) of environmental variables were used to assess collinearity. As no variables had
277 a VIF > 10 , none were excluded. A full CCA, with all environmental variables included, was first performed
278 to quantify the total amount of species–environment variance explained by the full set of variables. A
279 series of independent and partial CCAs with variance partitioning were performed to constrain analyses,
280 assess the relative explanatory power, and assess the unique and shared variance contributions of each
281 variable. Individual CCAs, of each variable alone, estimate the marginal (unconstrained) explanatory
282 power (i.e., how much variation a single variable explains when considered alone, without accounting
283 for correlations with other variables). Partial CCAs assess the unique (conditional) contribution of each
284 environmental variable after statistically controlling for all remaining variables. This analysis isolates the
285 variance uniquely attributable to each predictor and identifies variables whose explanatory power is
286 driven by covariation with others. Finally, variance partitioning was used to decompose the total
287 explained variation into unique and shared fractions, allowing assessment of how much variation was
288 due to individual predictors versus overlapping environmental gradients. Permutation test results ($p >$
289 0.05), CCA coefficients and lambda ratios (λ_1/λ_2) of the first constrained eigenvalue (λ_1) to the second
290 unconstrained eigenvalue (λ_2) were used to identify the environmental variables most appropriate for
291 quantitative inference models. As a guide, high λ_1/λ_2 ratios are necessary for a variable to have enough
292 explanatory power to be included in quantitative inference models (Ter Braak and Prentice 1988; Juggins
293 2013). All ordination analyses were performed using the *vegan* package version 2.7-1 (Oksanen et al.
294 2013) in R (R Core Team, 2024).

295

296 ML and iterations of inverse ($_{INV}$) and classical ($_{CLA}$) WA models with and without tolerance downweighting,
297 and WAPLS with up to five components were assessed to determine the best performing transfer

298 functions. These methods were applied because they capture different aspects of species–environment
299 relationships: WA provides a simple unimodal estimator; WAPLS allows more complex responses
300 through latent components; and ML emphasises taxa with narrow ecological tolerances. Using multiple
301 approaches therefore offers complementary strengths and helps identify the most reliable and robust
302 model through cross-validation. All models were performed with bootstrapping and 100 iterations. Model
303 R^2 , bootstrapped R^2 (R_{boot}^2), root mean square error (RMSE) and root mean square error of prediction
304 (RMSEP) values were used to assess performance. RMSEP and R_{boot}^2 performance was favoured over
305 R^2 and RMSE. RMSEP between WAPLS components was also used to assess overfitting. WA and
306 WAPLS-1 results are often similar as WAPLS is built upon on the same weighted-averaging framework
307 as WA (ter Braak and Juggins 1993). When this was the case and WAPLS components did not improve
308 performance, WA was favoured as the most parsimonious model. Software program C2 version 1.8
309 (Juggins 2003) was used to develop all transfer functions.

310 **3 Results**

311 **3.1 Lake water chemistry**

312 Analyses of 40 plateau lakes on Macquarie Island showed that lake water general parameters (EC, pH
313 and DO), and nutrients, did not vary significantly ($p > 0.01$) across the 2022 sampling events (E2-4; Table
314 1). Temperature varied, being significantly lower in E2 compared to E3 and E4 ($p < 0.01$). Lakes were
315 moderately acidic (pH 5.7) to alkaline (pH 9.14). Mean EC ranged from 126–261 $\mu\text{S cm}^{-1}$, with a decrease
316 in EC from west to east across the island. Lakes were oxic (DO = 8.64–12.61 mg L^{-1}) and oligotrophic,
317 with PO_4^{3-} and TON concentrations under or close to detection limits (< 0.01 – 0.02 mg L^{-1} and < 0.06 – 0.1
318 mg L^{-1} , respectively). Similarly, comparison with data from plateau lakes sampled in 2018 showed no
319 significant difference ($p > 0.01$) across all lake water general parameters, excluding temperature,
320 indicating generally stable conditions in plateau lakes across years. However, a comparison between
321 plateau lakes measured in 2022 and coastal lakes in 2006 did show significant differences ($p < 0.01$).
322 Coastal sites in 2006 were generally eutrophic with higher nutrient ranges (TON = 0.007–4.636 mg L^{-1}
323 and $\text{PO}_4^{3-} = 0.1$ – 9.9 mg L^{-1}), and higher EC (406–1482 $\mu\text{S cm}^{-1}$), while temperature, DO, pH, Si were
324 not significantly different ($p > 0.01$) (Table 1; see Supplementary Table S1 and S2 for full results).

325

326

327 Table 1: Summary of lake water general parameters and nutrient data. Temp. = temperature, DO = dissolved oxygen, EC =
 328 electrical conductivity, Si = silicate, PO₄³⁻ = phosphate, TON = total oxidised nitrogen.

	Temp. (°C)	DO (mg L ⁻¹)	EC (µs cm ⁻¹)	pH	Si (mg L ⁻¹)	TON (mg L ⁻¹)	PO ₄ ³⁻ (mg L ⁻¹)
2022							
Mean	8.7	11.59	188	7.03	0.648	0.06	0.00467
Min	6.4	8.69	135	5.65	0.100	0.06	0.00326
Max	16.1	12.95	267	9.15	4.333	0.10	0.02391
E1 mean (n=39)	7.6	12.47	188	7.02	0.767	0.06	0.00568
E2 mean (n=37)	9.1	11.94	197	7.03	0.611	0.06	0.00414
E3 mean (n=39)	9.6	10.48	177	7.05	0.515	0.06	0.00351
2018 (n=40)							
Mean	9.4	10.95	153	7.35	-	-	-
Min	6.8	8.56	101	5.99	-	-	-
Max	15.8	12.64	292	9.21	-	-	-
2006 (plateau) (n=5)							
Mean	6.4	11.59	192	6.92	0.047	0.00564	0.0070
Min	5.5	11.35	164	6.35	0.003	0.00004	0.0013
Max	7.4	11.80	224	7.46	0.092	0.02449	0.0155
2006 (coastal) (n=17)							
Mean	8.4	11.32	889	7.19	0.719	1.23331	1.124
Min	6.0	9.17	406	5.50	0.074	0.02430	0.007
Max	13.1	14.43	1482	8.13	2.706	9.89000	4.636

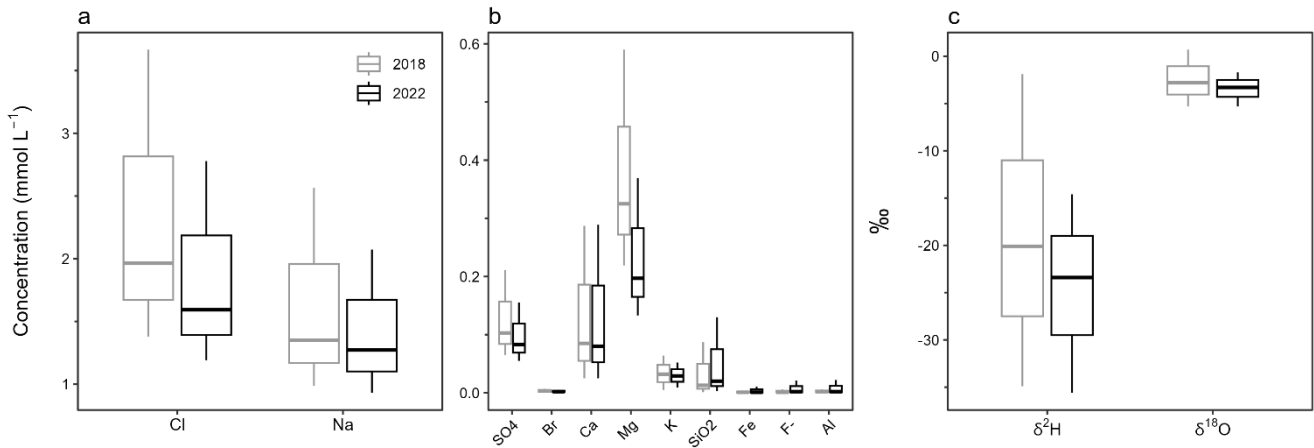
329

330 Major ion analysis of the 40 plateau lakes showed that, although dilute in concentration, Cl (1.1–3.7
 331 mmol L⁻¹) and Na (0.9–2.6 mmol L⁻¹) dominate the ionic composition of all lake waters (Fig. 3; see
 332 Supplementary Table S3 for full cation and anion results). All lakes showed similar ionic ratios to
 333 seawater for SO₄, Cl, Mg, and Na, suggesting a marine origin. Seawater ionic ratios diverged for K, Ca
 334 and F for some lakes, while SiO₂ was higher in all lakes, suggesting additional sources for these ions.
 335 (Fig. 4).

336

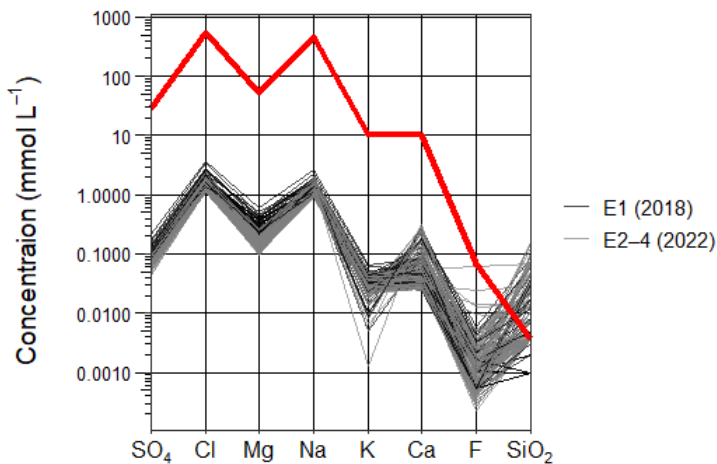
337 Statistical analyses showed no significant ($p > 0.005$) differences in major ion concentrations across 2022
 338 sampling events (E2–4). Broader changes were detected between 2018 and 2022, with Cl, SO₄, Br, and
 339 Mg all showing significantly higher mean concentrations ($p < 0.005$) in 2018 compared to all 2022

340 sampling events (E2–4). Fe, Na, K, Ca, F, SiO₂, and Al did not significantly vary ($p > 0.005$) between
341 sampling events. All ions that show significant variation ($p < 0.005$) have predominantly marine sources.



342

343 Fig. 3: Box and whisker plots showing the range and mean of 2018 and 2022 lake water major ions **a)** Cl and Na; **b)** SO₄, Br,
344 Ca, Mg, K, SiO₂, Fe, F⁻, and Al; and **c)** stable water isotopes δ²H and δ¹⁸O.

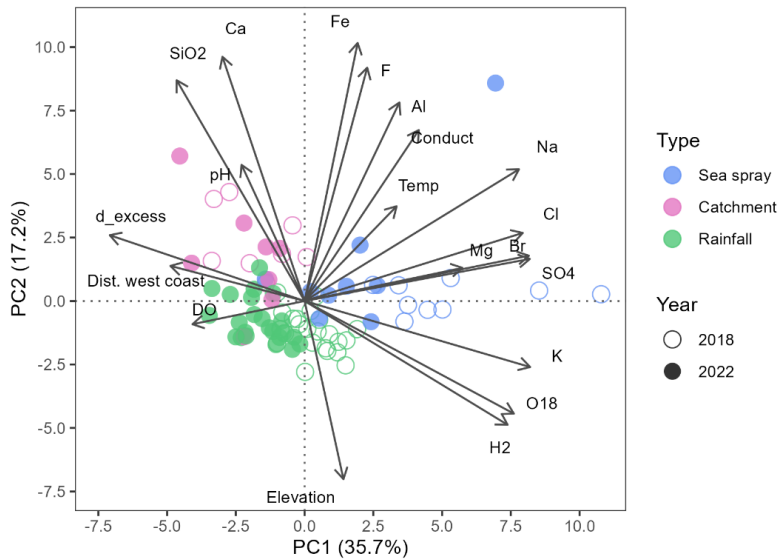


345

346 Fig. 4: Scholler plot comparing the ionic composition (SO₄, Cl, Mg, Na, K, Ca, F and SiO₂) of Macquarie Island lake waters and
347 seawater (red line), categorised into sampling years 2018 (black lines) and 2022 (grey lines).

348 PCA showed the relationship between lake water chemistry parameters, with samples grouped by lake
349 type and sampling year (Fig. 5). Together, PC1 and PC2 captured 53% of the total variance in the
350 dataset. PC1 represents a salinity and sea-spray gradient with variability in EC, distance from the west
351 coast, Na, Cl, Br, Ca, Mg, and K captured. PC2 represents an altitude and terrestrial ion gradient with

352 variability in elevation, temperature, SiO₂, Ca, Fe, and F captured. Lakes cluster according to
 353 environmental processes (groups derived from Meredith et al., 2022), with SSA influenced lakes having
 354 positive PC1 scores, which suggests higher concentrations of marine derived ions. The grouping of
 355 samples influenced by catchment processes and those influenced by rainfall is driven by PC2 with
 356 catchment influenced lakes having lower elevation and higher ion concentrations. SSA and rainfall
 357 influenced lakes cluster based on the year that they were sampled with greater ion concentrations in
 358 2018.

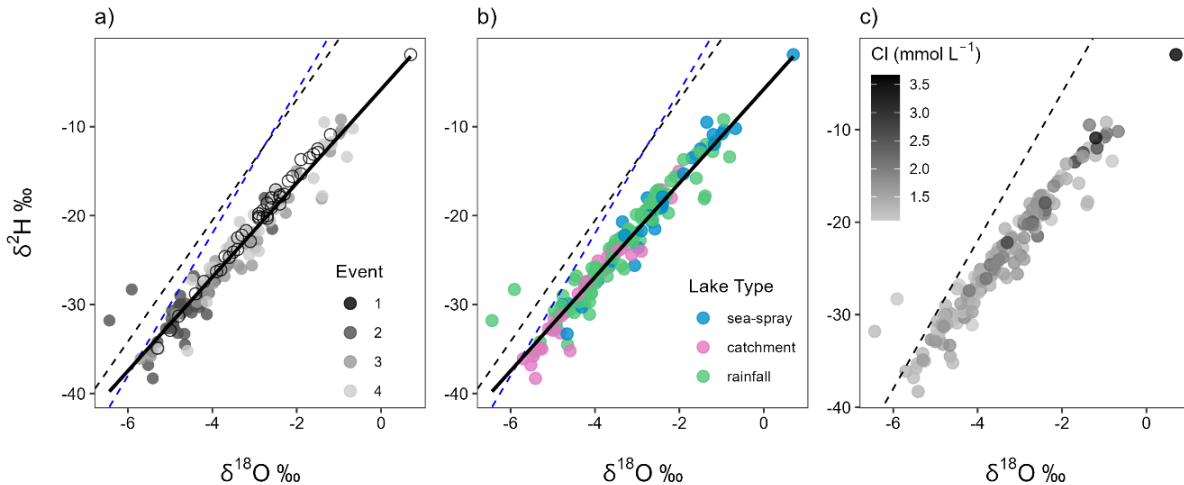


359
 360 Fig. 5: Principal Component Analysis (PCA) of Macquarie Island lake waters, showing the relationships between major ions and
 361 environmental parameters. Lakes are coloured by lake type, showing that lakes cluster based on the dominate geochemical
 362 processes identified by Meredith et al., (2022). Dist. west coast = distance from the west coast (m), Conduct = electrical
 363 conductivity.

364 3.2 Stable water isotopes

365 $\delta^2\text{H}$ and $\delta^{18}\text{O}$ were measured in the 2022 samples and ranged from -38.3 to -9.2‰ and -38.3‰ to -
 366 0.67‰, respectively. Lake waters in 2018 and 2022 fell below the Global and Cape Grim (northwest
 367 Tasmania) Meteoric Water Lines (MWLs), suggesting slight isotopic enrichment in Macquarie Island's
 368 lakes (Fig. 6). In 2018, lake waters were significantly higher in $\delta^2\text{H}$ (mean -24.8 ‰) and $\delta^{18}\text{O}$ (mean -
 369 2.83‰) compared to 2022 (mean $\delta^2\text{H}$ = -24.8 ‰ and $\delta^{18}\text{O}$ = -3.55 ‰). Significant isotopic enrichment of
 370 $\delta^2\text{H}$ and $\delta^{18}\text{O}$ ($p < 0.001$) can be seen in the data at the beginning of the 2022 austral summer (E2–3;
 371 Fig. 6a). SSA influenced lakes tended to have higher isotopic values, while catchment influenced lakes

372 had lower values (Fig. 6b), with a significant difference between all lake types detected ($p < 0.001$). LK20
 373 and LK21 from E2 were outliers, plotting above the MWLs with lower $\delta^{18}\text{O}$ values. Cl concentrations
 374 appeared to be related to $\delta^2\text{H}$ and $\delta^{18}\text{O}$ values (Fig. 6c), however the correlation between the parameters
 375 was low ($R^2 \leq 0.24$). This lack of relationship was consistent across lake types and sampling events.



376
 377 Fig. 6: Stable water isotope $\delta^2\text{H}$ and $\delta^{18}\text{O}$ differences in Macquarie Island lake waters, shown across: **a)** sampling events; **b)**
 378 lake type; **c)** $\delta^2\text{H}$ and $\delta^{18}\text{O}$ relationship shown with Cl concentration (mmol L^{-1}). Solid black line shows Macquarie Island
 379 regression, blue dashed line is the Global Meteoric Water Line (GMWL: $\delta^2\text{H} = 8 \delta^{18}\text{O} + 10$), and black dashed line is the Cape
 380 Grim Local Meteoric Water Line (LMWL: $\delta^2\text{H} = 6.8 \delta^{18}\text{O} + 6.65$).

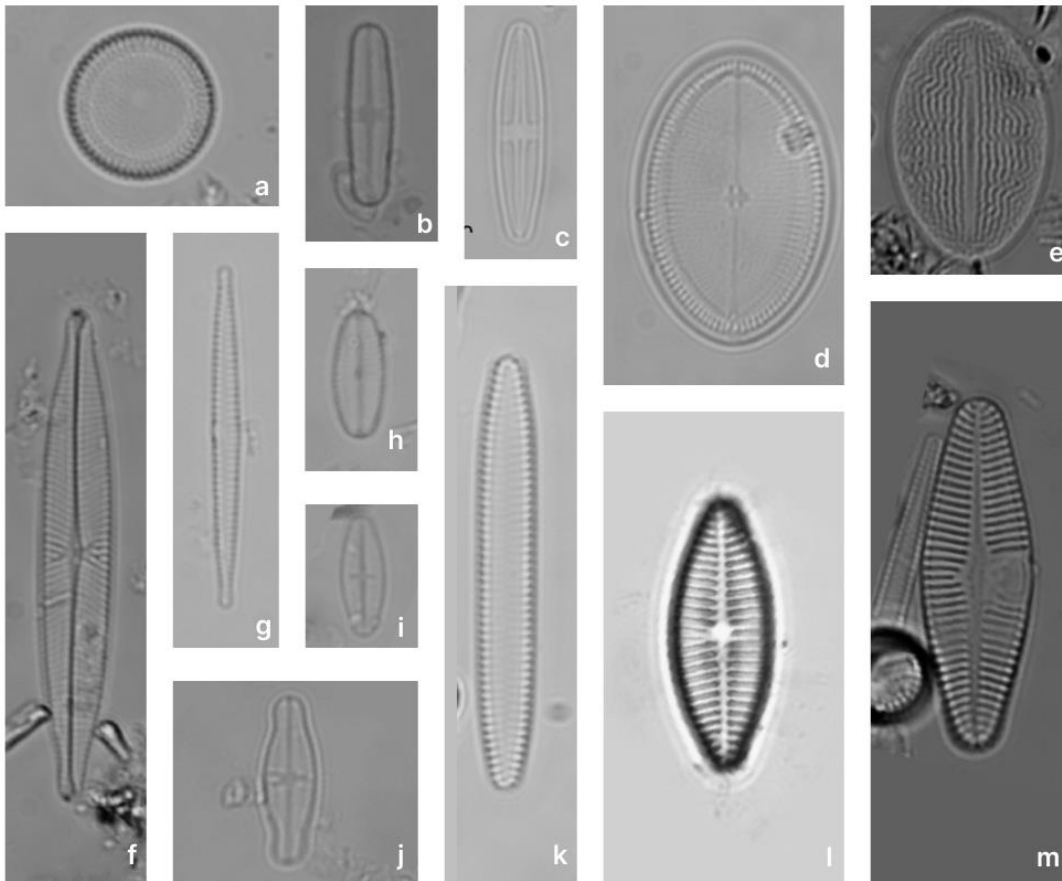
381 3.3 Diatoms

382 3.3.1 Diatom communities

383 In total, 141 diatom taxa from 45 genera were identified in the 52 plateau and coastal lakes. Ninety-six
 384 taxa (including 21 unknown species) from 30 genera remained in the dataset after taxa with $< 1\%$ relative
 385 abundance were excluded. The most taxon-rich genera were *Pinnularia* (16 taxa), *Psammothidium* (12
 386 taxa), and *Planothidium* (8 taxa). The most dominant taxa being both common, occurring in > 15 lakes,
 387 and abundant, occurring $> 25\%$ relative abundance in at least one sample, were *Aulacoseira principissa*
 388 Van de Vijver, *Psammothidium abundans* (Manguin) Bukhtiyarova & Round, *Psammothidium confusum*
 389 var. *atomoides* (Manguin) van de Vijver, unknown species 111, *Psammothidium confusum* (Manguin)
 390 van de Vijver, *Fragilaria capucina* Desmazières, and *Navicula bergstromiana* Vyverman et al. Coastal
 391 and plateau lakes showed distinctly different assemblages, with coastal lakes exhibiting less diversity
 392 (mean number of species = 20) and dominated by taxa including *F. capucina*, unknown sp. 111,

393 *Planothidium quadripunctatum* (D.R.Oppenheim) Sabbe, *Planothidium delicatum* (Kützing) Round &
 394 Bukhtiyarova, and *Planothidium lanceolatum* (Brébisson ex Kützing) Lange-Bertalot. Plateau lakes were
 395 more diverse (mean number of taxa = 40) and dominated by *A. principissa*, *P. abundans*, *P. confusum*
 396 var. *atomoides*, *P. confusum*, and *N. bergstromiana*, *Achnanthidium modestiformis* (Lange-Bertalot) Van
 397 de Vijver, *Cocconeis placentulata* Ehrenberg, and unknown species 21. No taxa were found in all lakes
 398 and none were uniquely restricted to either coastal or plateau lakes, although clear differences in species
 399 composition and relative abundance were observed. See Figure 7 for microscopy photos of the most
 400 abundant taxa.

10µm



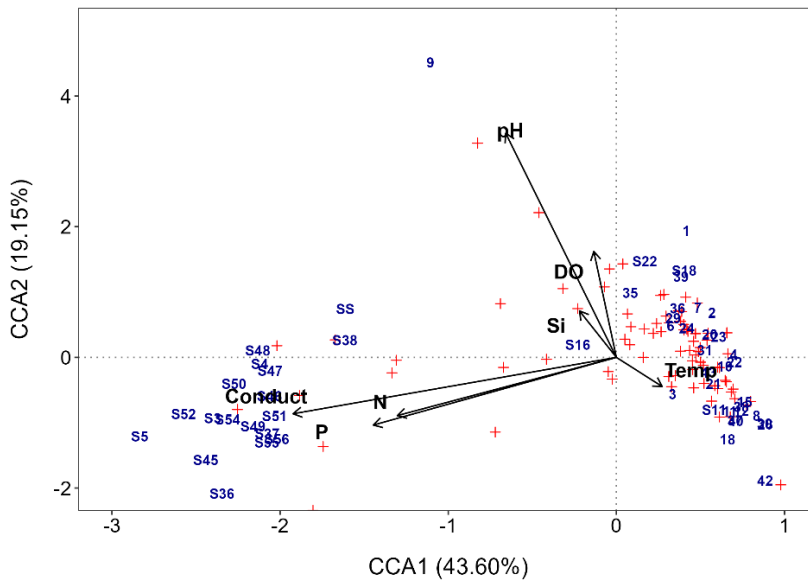
401
 402 Fig. 7: The most abundant diatom taxa from plateau and coastal lakes on Macquarie Island. **a)** *Aulacoseira principissa*; **b)**
 403 *Psammothidium abundans*; **c)** *Psammothidium confusum*; **d-e)** *Cocconeis placentulata*; **f)** *Navicula bergstromiana*; **g)** *Fragilaria*
 404 *capucina*; **h)** Unknown species 21; **i)** *Psammothidium confusum* var. *atomoides*; **j)** *Achnanthidium modestiformis*; **k)** Unknown
 405 species 111; **l)** *Planothidium delicatum*; **m)** *Planothidium lanceolatum*.

406 **3.3.2 Diatom-environment relationships**

407 The full CCA model was significant ($p = 0.001$), with environmental variables explaining 23.9% (Table 2)
 408 of the total variance in diatom species composition (constrained inertia = 1.5). Together, the first two
 409 canonical axes explained 62.8% of the total constrained variance (Table 2; Fig. 8). Forward selection
 410 with Bonferroni corrections, identified EC and pH ($p = 0.003$), and temperature ($p = 0.015$) as the most
 411 significant predictors of diatom community composition, collectively explaining 15.4% of the total
 412 variance. This equates to 70% of the total explained variance in the full model, capturing the major
 413 environmental gradients influencing species distribution with a more parsimonious model.

414 Table 2: Full CCA model results

Axis	Eigenvalue	Proportion of variance explained (%)	Cumulative proportion (%)
CCA1	0.77	51.07	51.07
CCA2	0.38	25.14	76.21
CCA3	0.22	14.55	90.76
CCA4	0.144	9.24	100.00
Constrained inertia	1.5		
Constrained proportion (%)	19.57		



415
 416 Fig. 8: Full CCA ordination biplot of diatom species and environmental data, numbers indicate sites, and grey symbols indicate
 417 diatom species. Si = silicate, P = phosphate, N = total oxidised nitrogen, and conduct = electrical conductivity (EC).

418 Individual CCAs were performed to assess the total explanatory power of each variable. EC and pH were
 419 shown to be the strongest, individually explaining 10.03% and 4.56% of the total variation, respectively.
 420 This corresponds to 45.83% and 20.86% of the total variance in the full CCA model. Additionally, EC
 421 was the only variable with a high λ_1/λ_2 ratio ($\lambda_1/\lambda_2 = 1.31$; Table 3), suggesting it is the only variable with
 422 enough explanatory power for inference modelling.

423

424 Table 3: Individual CCA results, independent CCAs run for each variable. (* = significant *p value* < 0.05)

Variable	λ_1 / λ_2	Constrained sum	Variance explained (%)	Proportion of full model explained (%)	p-value
Electrical conductivity	1.31	0.64	10.62	42.28	0.001*
Phosphate	0.73	0.40	6.59	26.23	0.001*
Total oxidised nitrogen	0.68	0.35	5.78	22.99	0.001*
pH	0.39	0.33	5.43	21.63	0.001*
Silicate	0.26	0.19	3.14	12.48	0.034*
Temperature	0.22	0.14	2.27	9.03	0.382
Dissolved oxygen	0.12	0.12	1.97	7.85	0.586

425

426 Partial CCAs were performed with each environmental variable tested separately while controlling for
 427 covariation with all other variables, to quantify unique and shared variance contributions. EC, pH, and Si
 428 were the only variables to have significant unique contributions ($p \leq 0.01$; Table 4). The shared and
 429 unique variance of each environmental variable is shown in Figure 9. EC explained the largest proportion
 430 of total constrained variation (46%) in diatom community composition, with a large shared component
 431 (17% unique, 28% shared), suggesting it acts along a major environmental gradient shared with TON
 432 and PO_4^{3-} (Fig. 8). Despite this, it performed well in all other CCAs and its unique contribution remained
 433 high, indicating it is an important independent driver of diatom structure across Macquarie Island lakes.
 434 Furthermore, low VIFs among all environmental variables (VIFs <3) indicated that multicollinearity was
 435 low. EC (VIF = 2.6) showed a low correlation with other variables ($R^2 \leq 0.47$), suggesting it represents a
 436 largely independent gradient in the dataset. In contrast, pH had similar unique variance (18.4%) and
 437 lower shared variance (2.4%), implying a more independent ecological influence.

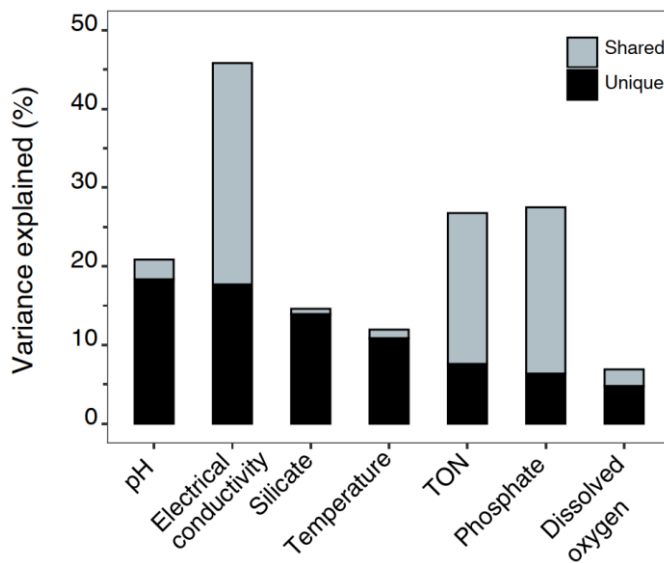
438

439

440

441 Table 4: Partial CCA results, where each variable was tested with the covariation of other variables controlled (* = significant p
 442 $value < 0.05$).

Variable	Variance explained (%)	Proportion of full model explained (%)	p-value
pH	5.97	18.92	0.001*
Electrical conductivity	5.58	17.62	0.001*
Silicate	3.87	11.99	0.008*
Temperature	2.81	8.61	0.151
Total oxidised nitrogen	2.06	6.28	0.651
Phosphate	1.71	5.20	0.774
Dissolved oxygen	1.34	4.06	0.991



443
 444 Fig. 9: Variance partitioning showing unique and shared proportions of variance explained by each environmental variable.

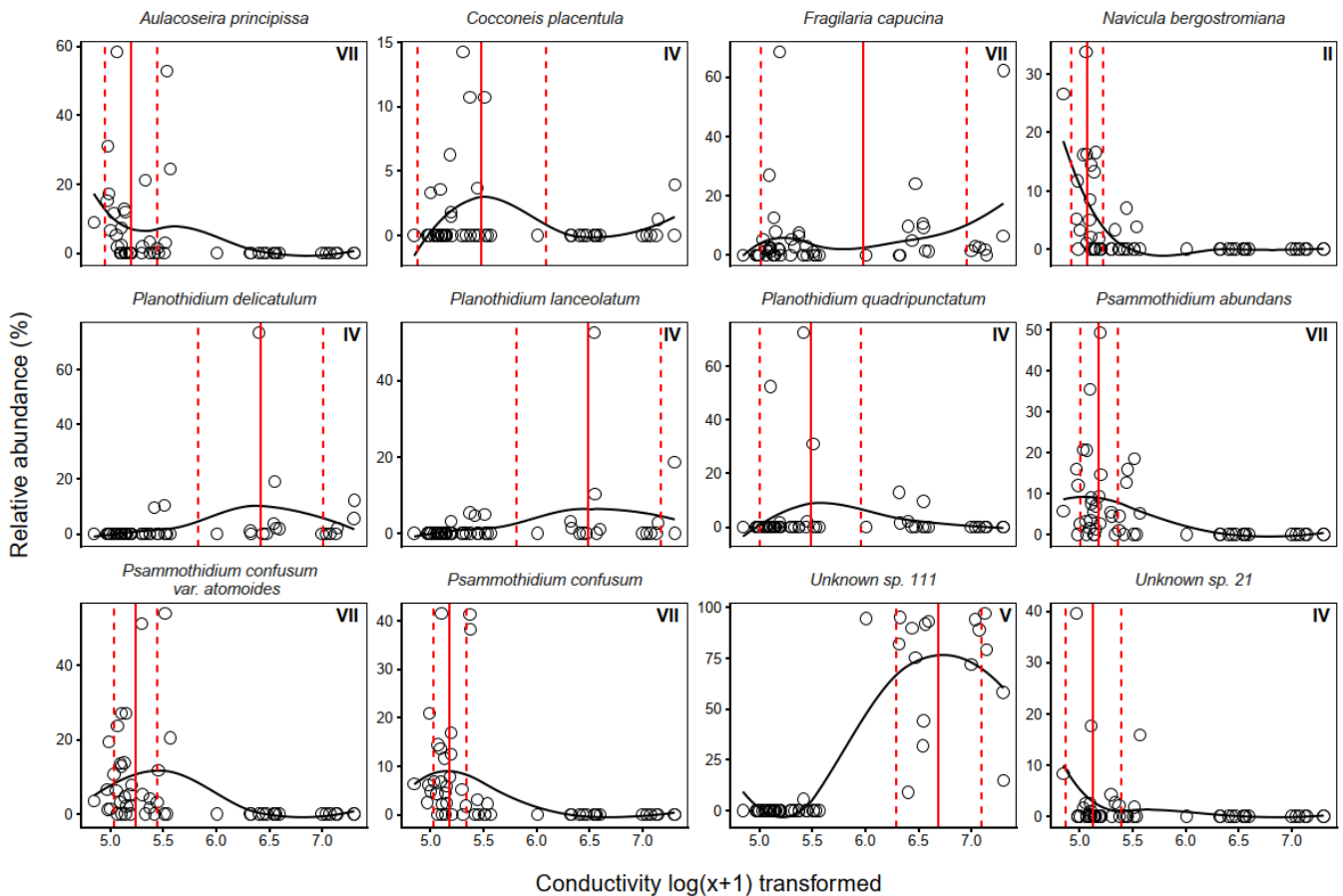
445 3.3.3 Species optima and tolerances

446 Species optima across major environmental gradients EC and pH were determined with WA. *F.*
 447 *capucina*, *P. lanceolataum*, and *P. delicatulum* were found across the EC range with broad tolerances,
 448 however each species showed different optima (Fig. 10). The apparent bimodal distribution of *F.*
 449 *capucina* likely reflects ecological plasticity across differing hydrochemical conditions and/or potential
 450 taxonomic aggregation within this morphotype. Exploration of a GAM-based response curve (Fig. S2)
 451 indicates *F. capucina* has a weak non-linear relationship with EC, suggesting a broad and flexible

452 ecological response rather than a strongly defined unimodal optimum. Unknown sp. 111 was found to
 453 tolerate high EC, while most other dominant species, including *A. principissa*, *C. placentulata*, *N.*
 454 *bergstromiana* and dominant *Psammothidium* species show tolerance and optima for low EC.

455

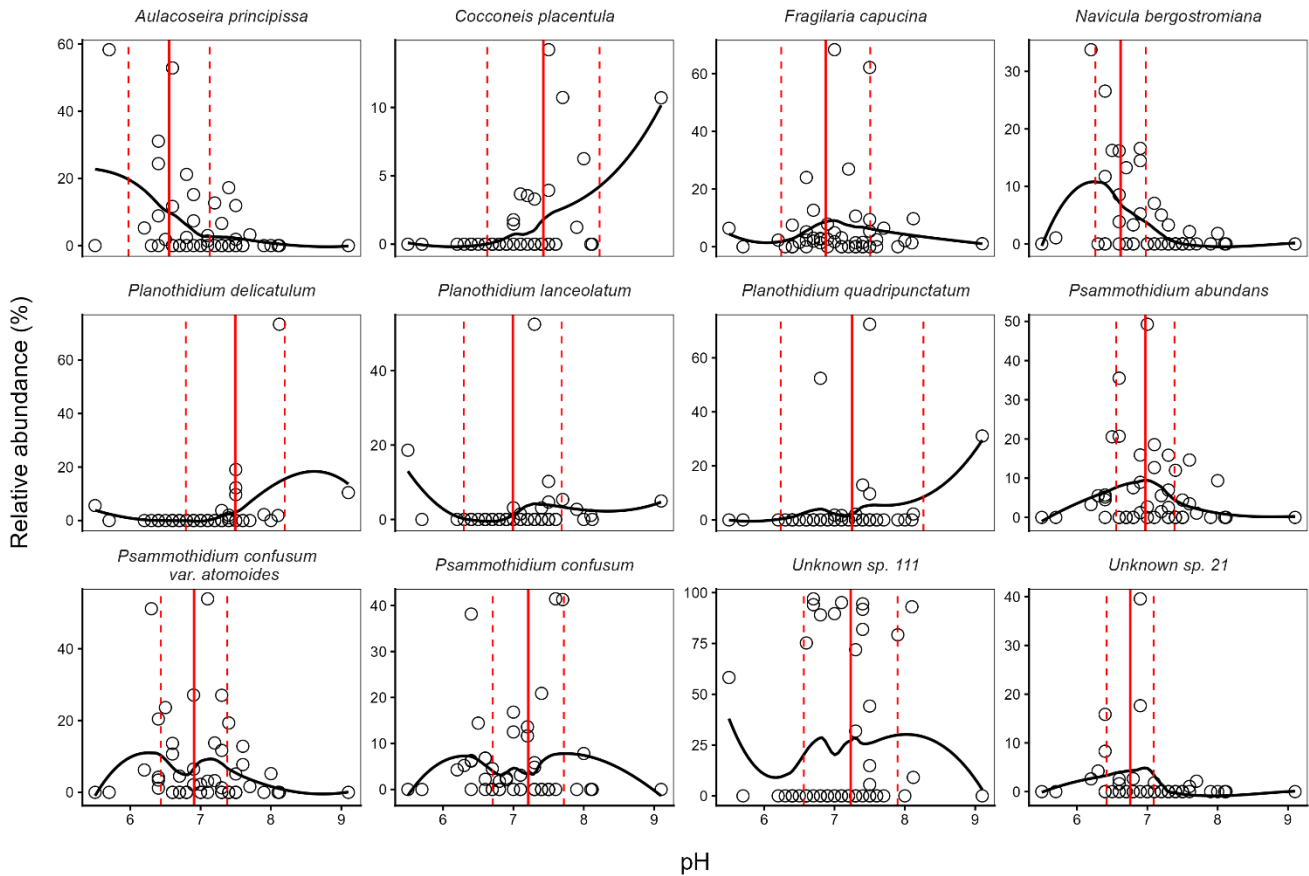
456 Dominant diatom species occurred across the pH gradient, with species optima ranging from moderately
 457 acidic to neutral (Fig. 11). Most dominant species had optima for moderate acidity, with *Psammothidium*
 458 species, *A. principissa*, and *N. bergstormiana* showing narrow pH tolerances. *C. placentulata* and *F.*
 459 *capucina* showed broader tolerances and unknown sp. 111 was the only dominant species with a near
 460 neutral optima.



461

462 Fig. 10: Weighted averaging (WA) electrical conductivity optima (solid red line) and tolerance ranges (dashed red lines) for
 463 dominant diatom species from Macquarie Island lakes. Observed relative abundances (%) are plotted against log-transformed
 464 conductivity, with fitted loess curves illustrating species response shapes along the conductivity gradient (126–1482 $\mu\text{S}/\text{cm}$).

465 Roman numerals indicate Gaussian response curve type.



466

467 Fig. 11: Weighted averaging (WA) pH optima (solid red line) and tolerance ranges (dashed red lines) for dominant diatom
 468 species from Macquarie Island lakes. Observed relative abundances (%) are plotted against pH, with fitted loess curves
 469 illustrating species response shapes along the pH gradient (5.50–9.14 °C).

470 3.3.4 Diatom transfer functions

471 Ordination analyses showed that EC and pH explained significant and independent proportions of
 472 variance in diatom composition. While temperature also showed significant but lesser contributions, it
 473 was not considered for transfer function development as diatom-based temperature reconstructions as
 474 species responses to temperature can be indirect and influenced by multiple co-varying environmental
 475 gradients, limiting the reliability of temperature inference (e.g. Juggins, 2013). While Si was shown to
 476 independently contribute to diatom variance, reduced CCA modelling with forward selection did not
 477 indicate it to be a major environmental gradient. Transfer functions were therefore only developed for EC

478 and pH. Transfer function results for the best performing WA, WAPLS, or ML model for EC and pH are
479 described in Table 5.

480
481 Table 5: Best performing WA, WAPLS or ML model results for electrical conductivity and pH.

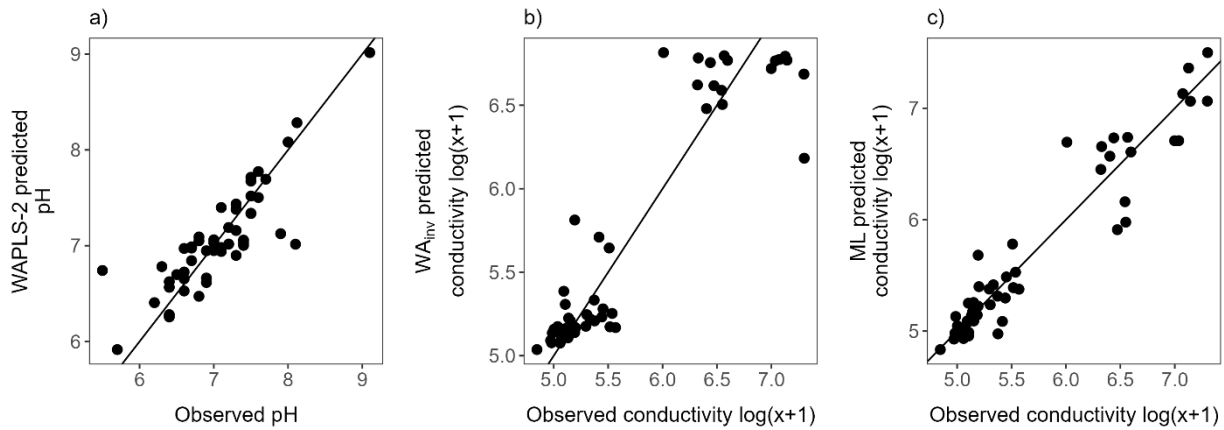
Variable	Model	R^2	R_{boot}^2	RMSE	RMSEP
Electrical conductivity	WA _{inv}	0.83	0.74	0.31	0.39
	ML	0.91	0.80	0.22	0.40
pH	WAPLS-2	0.72	0.26	0.33	0.60

482
483 For EC, WA_{INV} and WAPLS-1 produced near identical results. WA_{INV} was favoured as the simpler model
484 (WA_{INV}, $R^2= 0.83$, $R_{boot}^2= 0.74$, RMSE = 0.31, RMSEP = 0.39). Although WAPLS-2 to -5 increased R^2
485 and reduced RMSE, each successive component progressively increased RMSEP by 13-16%, thereby
486 reducing performance. Given the unimodal gradient structure of the dataset, ML modelling was also
487 assessed for EC. ML showed slightly stronger predictive performance to WA_{INV}, with higher R_{boot}^2 and
488 comparable RMSEP (ML, $R^2= 0.91$, $R_{boot}^2= 0.80$, RMSE = 0.23, RMSEP = 0.40).

489
490 Comparison of observed and predicted value scatter plots indicated that ML achieved a tighter fit, with
491 WA_{INV} showing increased predictive error at higher EC ranges (Fig. 12). However, further inspection
492 indicated that only ~30% of taxa displayed Gaussian (Type IV–V) response curves indicating ML may
493 not be the most appropriate approach (Fig. 9 and see Table S5 for full Gaussian response curve results).
494 However, overfitting from ML is not likely as RMSEP did not increase. Overall, both models show cross-
495 validated performance and are considered robust.

496
497 pH had poor performance across all WA and WAPLS models with high RMSEP (≥ 0.6) and low R_{boot}^2 (\leq
498 0.26). WAPLS-2 was found to be the strongest model (WAPL-2, $R^2= 0.72$, $R_{boot}^2= 0.26$, RMSE = 0.33,
499 RMSEP = 0.60). ML modelling showed poor performance for pH with high RMSEP = 0.93.

500



501

502 Fig. 12: Comparison of observed environmental measurements with values predicted by diatom-based transfer functions: **a)** pH estimated using
 503 WAPLS-2; **b)** conductivity estimated using WA with inverse deshrinking (WA_{INV}); and **c)** conductivity estimated using the maximum likelihood
 504 (ML) method. Black lines show the 1:1 line.

505 4 Discussion

506 4.1 Annual and seasonal lake water hydrogeochemical variation

507 The seasonal hydrochemistry dataset presented in this study support the 2018 baseline assessment
 508 (Meredith et al., 2022) that lake water chemistry is controlled by SSAs, terrestrial catchment processes,
 509 elevation and rainfall dilution. The seasonal water chemistry data, which is presented for the first time in
 510 this study, shows that there is no significant variation in major ions across the 2022–23 austral summer.
 511 Comparison of 2018 and 2022 data shows that significant variation ($p < 0.005$), in some major ions is
 512 evident, with higher concentrations in 2018 of Br and Cl, SO₄, and Mg associated with SSAs. Although
 513 not statistically significant ($p > 0.005$), other sea-spray derived ion mean values (Na, Ca, K) were higher
 514 in 2018 (Fig. 3; Table S4). However, not all ions increased in concentration, and terrestrially derived ions
 515 such as Fe, F, Si, and Al were lower in 2018, suggesting that lakes in 2022 had stronger SSA influence.
 516

517 Despite these changes, PCA of the 2018 and 2022 lake water chemistry datasets (Fig. 5) show that
 518 lakes typically cluster by the lake types identified in Meredith et al. (2022) (i.e., as SSA, catchment and
 519 rainfall influenced). This indicates that the major hydrogeochemical processes influencing Macquarie
 520 Island lakes are consistent between years, with no major environmental shifts occurring in weathering
 521 and erosion of the island's geology, suggesting these processes are stable on an annual time scale.

522 Identifying hydrogeochemical stability is important for identifying lake sites suitable for diatom–
523 conductivity inference models. It also strengthens palaeoclimate interpretations by suggesting that local
524 lake dynamics are relatively constant, supporting the hypothesis that in sea-spray dominated lakes,
525 proxies primarily record externally forced changes driven by the SHW rather than internal hydrological
526 or geochemical dynamics (Saunders et al. 2018; Perren et al. 2020). This further emphasises that water
527 chemistry characteristics are critical to consider in site-selection, to develop reliable SHW
528 reconstructions on Macquarie Island.

529 **4.2 Evaporation**

530 Interpreting environmental proxies as direct indicators of climate variability can be challenging, as
531 multiple processes may produce similar signals (Molén 2024). When using diatom–conductivity models
532 to infer past SHW variability, it is essential to consider how near surface evaporation has the potential to
533 concentrate ions in surface waters and mimic the effects of other processes such as increasing lake
534 water salinity from SSA deposition due to stronger winds. Although this study and previous studies
535 (Evans 1970; Buckney and Tyler 1974; Meredith et al. 2022) have demonstrated that SHW-driven SSA
536 inputs are a dominant control on lake water chemistry on Macquarie Island, the role of evaporation in
537 amplifying these signals remains unclear.

538

539 To explore this, we analysed $\delta^2\text{H}$ and $\delta^{18}\text{O}$ values from 2018 and across the 2022–23 Austral summer.
540 Isotopic enrichment is evident across the 2022–23 season (Fig. 6a), indicating a strengthening
541 evaporative signal through summer. Lake stable water isotopes sampled in 2018 were significantly more
542 enriched than the 2022 mean, as expected given that the 2018 samples were collected in late summer,
543 when evaporative effects are strongest and cumulative due to warmer temperatures throughout summer.
544 This is supported by lake water temperatures being significantly lower in early summer (E2) compared
545 to late summer (E3 and E4; Table 1). Given Macquarie Island’s persistently high cloud cover, humidity,
546 and low sunshine hours (BOM, 2025), solar evaporation is likely limited and confined to the summer
547 season. Evaporation can produce heavy-isotope enrichment and the residual lake water becomes
548 progressively enriched in heavier isotopes ($\delta^2\text{H}$ and $\delta^{18}\text{O}$), moving away from the Global MWL (Gat 1996).
549 Comparisons between E1 (2018) and E4 (2022), which were sampled at the same time of the year in
550 January–February provide a valuable comparison of potential interannual variability in lake water
551 chemistry and processes (Fig. 3, Table S4). These two sampling events show near identical mean

552 isotopic composition ($p > 0.01$; $\delta^2\text{H} = -20.7\text{‰}$ and $\delta^{18}\text{O} = -2.8\text{‰}$ in 2022, and $\delta^2\text{H} = -20.1\text{‰}$ and $\delta^{18}\text{O} = -$
553 2.8‰ in 2018), suggesting broadly stable summer evaporative conditions between years. Furthermore,
554 SSA influenced lakes on the plateau are in proximity to the west coast and have the greatest exposure
555 to the SHW (Fig. 2b). These lakes have significantly higher isotopic enrichment (Fig. 5b), providing
556 further evidence that wind is likely the primary driver of evaporation in plateau lake waters across
557 Macquarie Island, particularly in lakes located on the west coast, which may be most suitable for
558 reconstructions of SHW dynamics (Saunders et al., 2018). As both wind-enhanced evaporation and
559 wind-driven SSA transport and deposition contributes to the concentration of SSA ions in these lakes,
560 both ion deposition and the concentration reflect a SHW signal.

561

562 Cl^- is a robust tracer of hydrogeochemical processes and, together with $\delta^2\text{H}$ and $\delta^{18}\text{O}$ values, can be
563 used to better understand evaporation (Kirchner et al., 2010). While the isotopic enrichment observed
564 generally indicates an evaporative signal, the absence of a correlation between Cl^- and $\delta^2\text{H}$ or $\delta^{18}\text{O}$ (Fig.
565 6c) suggests that isotopes are capturing short-term (summer) evaporation rather than sustained
566 evaporative concentration sufficient to increase Cl^- concentration in the lake waters like those in
567 environments driven primarily by solar evaporation (Meredith et al. 2009). On Macquarie Island, wind-
568 driven SSA deposition and rainfall dilution therefore likely remain the primary drivers of Cl^- variability.
569 Consequently, EC in lake waters of Macquarie Island remains a robust proxy for interpreting variations
570 in SHW strength.

571 **4.3 Diatom communities**

572 Diatom analysis showed that typical sub-Antarctic genera (Van de Vijver 2019; Goeyers et al. 2022),
573 including *Psammothidium*, *Planothidium*, and *Fragilaria*, dominated lake diatom communities on
574 Macquarie Island. Across 52 lakes, 141 taxa were identified, indicating intermediate species diversity
575 relative to previous studies on the island which reported 102 (McBride, 2009) and 208 (Saunders et al.,
576 2009) species. Consistent with these earlier studies we have demonstrated that diatoms on Macquarie
577 Island exhibit clear and distinct ecological preferences. Combined with the pronounced environmental
578 gradients among lakes, these species-environment relationships provide a strong basis for using diatoms
579 as indicators of limnological conditions and environmental change.

580

581 *Psammothidium* species are characteristic of low EC sites (Van de Vijer et al. 2002), and while
582 abundance and dominance of key *Psammothidium* species showed variation along the lower end of the
583 EC gradient (Fig. 10), they dominated low EC sites. *N. bergstromiana* is considered endemic to
584 Macquarie Island and was commonly found with dominant *Psammothidium* species at low EC sites,
585 typically occurring where EC was $<200 \mu\text{S cm}^{-1}$, consistent with what has previously been reported
586 (Sabbe et al. 2019). *A. principissa*, previously identified as *Aulacoseria distans* (Ehrenberg) Simonsen
587 on Macquarie Island (McBride, 2009; Saunders et al., 2009), was also common at low EC (Fig. 10). This
588 taxa is commonly found on sub-Antarctic Islands and is suggested to prefer very low conductance values
589 $<80 \mu\text{S cm}^{-1}$ (Van de Vijver 2012), while EC was not observed $< 160 \mu\text{S cm}^{-1}$ in this dataset, *A. principissa*
590 may be an indicator of very low EC conditions.

591

592 *P. lanceolatum* was a dominant high EC, high nutrient taxa. While it has been found to dominate flora
593 elsewhere, this contrasts previous studies where it has been reported to be characteristic of oligotrophic
594 conditions (Van de Vijer et al. 2002). *F. capucina*, *P. delicatulum*, and unknown sp. 111 were more
595 commonly dominant at high EC. *F. capucina* was found across the EC gradient displaying a bimodal
596 distribution (Fig. 10), consistent with its cosmopolitan and ecologically tolerant nature (Van de Vijer et
597 al., 2002).

598 **4.4 Developing transfer functions**

599 A key aim of this study was to update and improve existing quantitative diatom models for Macquarie
600 Island. While the dominant taxa identified here are consistent with those reported by Saunders et al.
601 (2009), the strength of some diatom–environment relationships differ. EC and pH remain strong
602 explanatory variables for diatom variation, whereas PO_4^{3-} and Si showed limited influence in the present
603 study (Table 3 and 4). This reduced explanatory power likely reflects the low nutrient variability across
604 plateau lakes, where concentrations were generally below detection limits.

605

606 Sub-Antarctic lakes are characteristically oligotrophic; high nutrient levels do occur, but they are
607 associated with peatlands or animal colonies, as is the case with coastal lakes on Macquarie Island
608 (Selkirk et al. 1990). Saunders et al. (2009) recorded greater nutrient variability across plateau sites at
609 the lower end of the EC gradient, attributed to enhanced organic inputs during periods of high ecological
610 disturbance from invasive rabbits. These differences suggest that the dataset in the present study

611 represents post-eradication limnological conditions that are more reflective of pre-invasion or near-
612 natural states, providing an updated basis for developing robust diatom–environment models that are
613 less influenced by disturbance. The use of field parameters collected across multiple sampling events
614 increases confidence that the developed models reflect representative environmental conditions
615 (Goldenberg Vilar et al. 2018; Kennedy and Buckley 2021). Such repeated-sampling approaches are
616 rarely achieved in diatom transfer function development, particularly in remote regions such as the sub-
617 Antarctic.

618

619 Widespread recovery of vegetation communities provides evidence for catchment scale ecosystem
620 recovery across the island (Springer 2018; Fitzgerald et al. 2021). While quantitative runoff or nutrient
621 time series are not available to directly extend this to limnological conditions, we are able to provide site-
622 specific evidence from one sedimentary diatom record. At Emerald Lake (LK6), downcore diatom
623 assemblages show a clear ecological shift coincident with the introduction of rabbits (1878 CE) and their
624 establishment on Macquarie Island, with *F. capucina* and *P. abundans* dominating downcore intervals
625 (Saunders et al. 2013). In contrast, diatom assemblages in recent (2022) surface sediments from this
626 site exhibit higher diversity (48 species) and greater similarity in assemblage composition to pre-rabbit
627 sediment intervals rather than assemblages from previously collected 2006 surface sediments (15
628 species), which were dominated by *F. capucina* (48% relative abundance). Notably, *F. capucina* was
629 absent from the 2022 surface sample. Together, these lines of evidence suggest that the modern
630 calibration dataset is less influenced by organic inputs and erosion associated with the rabbit invasion
631 period. Accordingly, we interpret the 2022 dataset as representing post-eradication recovery conditions
632 that are moving toward, but do not necessarily fully reflect, pre-disturbance baseline states. However,
633 further studies are needed to assess how widespread this is across the island.

634

635 EC was shown to be the major independent driver of diatom assemblages, with strong performance in
636 all CCA models, individually accounting for almost 50% of the variance in the full CCA model and strong
637 explanatory power as indicated by λ_1/λ_2 (Table 3). Although EC reflects a high proportion of shared
638 variance (Fig. 9), this is consistent with its role as an integrative measure of ionic strength and catchment
639 inputs. The shared component primarily reflects its covariation with major ions and nutrient variables
640 (TON and PO_4^{3-}), which are typically correlated with EC in these systems. Despite this overlap, EC

641 retained a strong and highly significant independent effect ($p = 0.001$), confirming its dominant ecological
642 influence on diatom distributions.

643

644 While PO_4^{3-} , TON, and Si each explained significant but moderate portions of individual variance (Table
645 3), they were no longer significant once covariation was controlled for (Table 4), meaning their
646 explanatory power is mostly shared variance with other environmental gradients, primarily EC and each
647 other, with negligible unique variance. This interpretation is supported by simple linear correlations
648 between EC and nutrient variables in coastal lakes, which show weak or absent relationships (Fig. S3).
649 These results indicate that although nutrients and EC co-occur in coastal systems, nutrient variability is
650 not strongly or systematically coupled to EC. Together with the VIFs (<3), variance partitioning and partial
651 CCA results (Table 4), this supports the interpretation that the weak unique nutrient signal reflects an
652 ecological reality in which EC exerts a first-order control on diatom assemblages, rather than a statistical
653 artefact of collinearity. Similarly, while pH explained a major and independent gradient in diatom variation
654 within plateau lakes (Fig. 8), it did not capture assemblage changes across high-EC, high-nutrient sites.
655 This was indicated by individual CCA results, which were less than half of the variance explained by EC
656 (Table 3). This, paired with the widespread oligotrophic nature of plateau lakes on Macquarie Island
657 lends strength to the independent explanatory power of EC across the whole dataset.

658

659 Furthermore, pH showed poor predictive performance as a transfer function, with the lowest $R_{boot}^2 = 0.26$,
660 and highest RMSEP = 0.6 from the WAPLS-2 model (Table 5). While this is surprising due to the strong
661 pH gradient across plateau sites, most diatoms were found across the pH gradient (Fig. 11) with some
662 species showing broad tolerance and pH ranges. EC had the strongest performance with the WA and
663 ML models producing the highest R_{boot}^2 (0.74 and 0.80, respectively) and comparable RMSEP. WA_{inv}
664 and WAPLS-1 showed identical performance, with no benefit from additional WAPLS components, which
665 progressively increased predictive error and decreased R_{boot}^2 , suggesting overfitting. WA was therefore
666 chosen over WAPLS as the simpler model.

667

668 The WA EC transfer function performed better than the previously published Macquarie Island diatom-
669 conductivity transfer function (Saunders et al., 2009), with higher R_{boot}^2 . However, some caution is
670 warranted when predicting across the upper EC range, where greater predictive error is evident (Fig.

671 12). This can be attributed to lower species turnover, higher variability in PO_4^{3-} , TON, and Si, and fewer
672 sites at the upper end of the nutrient and EC gradients. Further refinement of the EC transfer functions
673 could be achieved with more evenly distributed sampling across the environmental gradient. The ML
674 model, with higher R_{boot}^2 , appears more capable of addressing these issues and maintains more
675 consistent predictive power across the EC range. This is likely due to its explicit curve-fitting approach.
676 By estimating individual species optima and tolerances, ML can better represent asymmetric or skewed
677 response curves (Birks 2012). The ML transfer function is therefore considered to be the preferred model,
678 although both WA and ML are robust based on comparable RMSEP.

679 **4.5 Future applications for reconstructing past climate changes**

680 The conceptual link between large-scale wind regimes and long-term limnological and ecological
681 responses in Southern Hemisphere lake systems is well established in previous studies (e.g., Saunders
682 et al. 2009; 2016; 2018; Perren et al. 2020, 2025; Van Nieuwenhuyze 2020; Humphries et al. 2021;
683 Meredith et al. 2022). The data presented here builds on this existing framework, and demonstrates that
684 incorporating diatom data with seasonal and multi-year hydrogeochemical data provides a unique
685 opportunity to comprehensively understand diatom–environment responses. By quantifying temporal
686 variability in hydrogeochemical processes, including the role of evaporation, this study strengthens
687 confidence that EC reflects SHW-driven sea-spray inputs rather than local lake hydrogeochemical
688 processes. This hydrological context is critical for interpreting diatom–environment relationships and
689 ensuring the reliability of EC as a proxy for past SHW behaviour, providing a strong foundation for future
690 palaeoclimate reconstructions. The resulting diatom–conductivity model provides a robust and
691 ecologically grounded framework for reconstructing long-term SHW variability on Macquarie Island and
692 establishes an important benchmark for sub-Antarctic palaeoclimate comparisons across the region.
693 This model will be applied in future studies to reconstruct past variability in the SHW and associated
694 hydroclimatic changes on Macquarie Island. Any future time-series monitoring of lake EC paired with
695 local wind speed records would further allow direct assessment of the relationship between wind speed
696 and lake salinity, including the rate of hydrogeochemical response and any wind speed thresholds
697 required to drive measurable change.

698

699 By capturing post-eradication and near-natural ecological conditions, the EC model developed in this
700 study offers an improved foundation for assessing long-term wind-driven variability, as it reduces

701 ecological noise associated with past disturbance. When applied in parallel with other proxies, such as
702 isotopic or geochemical indicators, these reconstructions will contribute to a more comprehensive
703 understanding of past SHW dynamics and their role in modulating Southern Hemisphere mid-high
704 latitude climate, thereby providing context for understanding future changes.

705

706 Furthermore, a multiproxy approach will be valuable for independently reconstructing key climatic
707 drivers, including precipitation, temperature, and atmospheric circulation, thereby improving
708 interpretations of past SHW variability and helping to assess how hydroclimatic processes may modify
709 EC signals (e.g., through dilution and enrichment). On Macquarie Island, geochemical indicators of sea-
710 spray and dust inputs (e.g., S, Br, Ti) can help distinguish marine aerosol delivery from catchment-
711 derived material, while glycerol dialkyl glycerol tetraethers (GDGT)-biomarker reconstructions can
712 provide an independent constraint on temperature variability. Both approaches are currently being
713 undertaken on Macquarie Island lake sediment cores by our research group. Mercury (Hg)
714 concentrations and isotopes offer an independent proxies for atmospheric transport and Hg deposition
715 linked to large-scale circulation, precipitation, and the influence of seabirds, all particularly well suited to
716 the remote setting of Macquarie Island (Schneider et al., 2022; Guédron et al., 2020), this is also the
717 focus of ongoing work (e.g. Schneider et al., 2024; Li et al., 2025). Although isotope ($\delta^2\text{H}$, $\delta^{18}\text{O}$) palaeo-
718 records are not currently available for Macquarie Island, they represent an important avenue for future
719 research to constrain precipitation–evaporation balance. Together, these complementary proxies
720 provide a framework to separate the relative influence of atmospheric circulation, hydroclimate, and
721 temperature on lake systems, providing more comprehensive palaeoclimate records and interpretations.

722 **5 Conclusion**

723 This study aimed to update and re-evaluate the reliability of diatom–conductivity models as a proxy for
724 reconstructing SHW variability on Macquarie Island by analysing diatom–environment relationships in
725 the context of seasonal and multi-year water chemistry and isotopic analyses. Our results demonstrate
726 that although lake hydrogeochemical processes vary locally, they remain stable seasonally and between
727 years. Lakes near the west coast and on the western edge consistently reflect strong SSA influence, and
728 while short-term evaporative enrichment occurs during summer, it does not obscure the dominant signal
729 of SHW-driven SSA inputs. Accordingly, EC reliably reflects SSA deposition rather than internal lake

730 hydrogeochemical processes, providing a firm mechanistic basis for the use of EC as an indicator of
731 SSA deposition in palaeoclimate studies on Macquarie Island.

732

733 Diatom–environment relationships were found to be strong and ecologically coherent, supporting the
734 development of a robust diatom–conductivity transfer function. Importantly, this study highlights the need
735 for careful site selection, with lakes that demonstrate stable hydrogeochemical behaviour, clear SSA
736 influence, and limited local disturbance providing the most reliable archives for reconstructing past SHW
737 variability. The resulting transfer function offers a reliable tool for reconstructing long-term SHW
738 dynamics, supported by well-characterised modern hydrological controls. Together, these findings
739 establish Macquarie Island as a well-constrained system for SHW reconstructions and provide a strong
740 foundation for future palaeoclimate work across the sub-Antarctic region.

741

742 **Supplementary material**

743 The Diatom Catalogue and Species List can be accessed from DOI [10.5281/zenodo.18041221](https://doi.org/10.5281/zenodo.18041221)

744

745 **Data availability**

746 The raw data supporting the conclusion on this work is available on request.

747

748 **Author contributions**

749 Caitlin Selfe: Conceptualization; Data curation; Formal analysis; Investigation; Methodology; Validation;
750 Visualization; Writing - original draft; Writing - review & editing.

751 Karina Meredith: Supervision; Research design; Resources; Writing - review & editing

752 Liza McDonough: Resources; Writing - review & editing

753 Justine Shaw: Supervision; Writing - review & editing

754 Stephen Roberts: Supervision; Writing - review & editing

755 Krystyna Saunders: Conceptualisation; Supervision; Resources; Funding acquisition; Writing - review
756 & editing

757 Competing interests: The contact author has declared that none of the authors has any competing
758 interests.

759

760

761 **Acknowledgments**

762 This work was supported by ARC SRIEAS Grant SR200100005 Securing Antarctica's Environmental
763 Future. CS was supported by an AINSE Ltd. Residential Student Scholarship and acknowledges help
764 undertaking fieldwork from Maggie Smith, Sam Beale, Jez Bird, and Adam Darragh. We thank the
765 Tasmanian Parks and Wildlife Service and Australian Antarctic Division (AAS 4628) for field support
766 and access to Macquarie Island. We also thank ANSTO laboratories for sample analysis, particularly
767 Chris Vardanega and Henri Wong. This work contributes to delivering the Australian Antarctic Science
768 Decadal Strategy, in particular the Climate System and Change key priority.

769 **References**

- 770 Andersen, T., J. Carstensen, E. Hernandez-Garcia and C. M. Duarte. Ecological thresholds and regime shifts: approaches to
771 identification. *Trends in Ecology & Evolution* 24 (1): 49-57. 2009.
- 772
- 773 Birks, H., D. Frey and E. Deevey. Numerical tools in palaeolimnology-progress, potentialities, and problems. *Journal of*
774 *paleolimnology* 20: 307-332. 1998.
- 775
- 776 Birks, H. J. B. Overview of numerical methods in palaeolimnology. In *Tracking environmental change using Lake sediments:*
777 *Data handling and numerical techniques, 19-92: Springer.* 2012.
- 778
- 779 BOM. Australian Bureau of Meterology, Climate statistics for Australian locations.
780 https://www.bom.gov.au/climate/averages/tables/cw_300004.shtml. 2025.
- 781
- 782 Buckney, R. T. and P. A. Tyler. Reconnaissance limnology of Sub-Antarctic islands. II. Additional features of the chemistry
783 of Macquarie Island lakes and tarns. *Marine and Freshwater Research* 25 (1): 89-95. 1974.
- 784
- 785 Chau, J. H., C. Born, M. A. McGeoch, D. Bergstrom, J. Shaw, A. Terauds, M. Mairal, J. J. Le Roux and B. Jansen van Vuuren.
786 The influence of landscape, climate and history on spatial genetic patterns in keystone plants (*Azorella*) on sub-Antarctic
787 islands. *Molecular Ecology* 28 (14): 3291-3305. doi: <https://doi.org/10.1111/mec.15147>. 2019.
- 788
- 789 Deng, Y. N., S. J. Roberts, K. M. Saunders, B. Perren and C. Selfe. Late-Holocene palaeoecological reconstruction of Southern
790 Hemisphere Westerlies variability on Subantarctic Macquarie Island. *The Holocene*: 09596836261432461. 2025.
- 791
- 792 Evans, A. J. Some aspects of the ecology of a calenoid copepod, *Psuedoboekela brevicaudata*. Brady, 1875, on a subantarctic
793 island. ANARE Scientific Reports, series B, 1, Zoology: 100. 1970.
- 794
- 795 Farqan, M., L. Xiang, J. Deng, H. Chen, W. Wang, S. Yu, Z. Zhu, C. Yan, C. Huang and X. Liu. Modern surface sediment
796 diatom assemblages and conductivity modeling in northern China. *Ecological Indicators* 179: 114229. 2025.
- 797
- 798 Fitzgerald, N. B., J. B. Kirkpatrick and J. J. Scott. Rephotography, permanent plots and remote sensing data provide varying
799 insights on vegetation change on subantarctic Macquarie Island, 1980–2015. *Austral Ecology* 46 (5): 762-775. 2021.
- 800

801 Fletcher, M.-S., J. Pedro, T. Hall, M. Mariani, J. A. Alexander, K. Beck, M. Blaauw, D. A. Hodgson, H. Heijnis and P. S.
802 Gadd. Northward shift of the southern westerlies during the Antarctic Cold Reversal. *Quaternary Science Reviews* 271:
803 107189. 2021.
804
805 Fogt, R. L. and G. J. Marshall. The Southern Annular Mode: variability, trends, and climate impacts across the Southern
806 Hemisphere. *Wiley Interdisciplinary Reviews: Climate Change* 11 (4): e652. 2020.
807
808 Gasse, F., P. Barker, P. A. Gell, S. C. Fritz and F. Chalie. Diatom-inferred salinity in palaeolakes: an indirect tracer of climate
809 change. *Quaternary Science Reviews* 16 (6): 547-563. 1997.
810
811 Gat, J. R. Oxygen and hydrogen isotopes in the hydrologic cycle. *Annual Review of Earth and Planetary Sciences* 24 (1): 225-
812 262. 1996.
813
814 Gillett, N. P., T. D. Kell and P. Jones. Regional climate impacts of the Southern Annular Mode. *Geophysical Research Letters*
815 33 (23). 2006.
816
817 Goeyers, C., D. H. Vitt and B. Van de Vijver. Taxonomic and biogeographical analysis of diatom assemblages from historic
818 bryophyte samples from Campbell Island (sub-Antarctic). *Plant Ecology and Evolution* 155 (1): 107-122. 2022.
819
820 Goldenberg Vilar, A., T. Donders, A. Cvetkoska and F. Wagner-Cremer. Seasonality modulates the predictive skills of diatom
821 based salinity transfer functions. *PLOS ONE* 13 (11): e0199343. doi: 10.1371/journal.pone.0199343. 2018.
822
823 Goyal, R., A. Sen Gupta, M. Jucker and M. H. England. Historical and projected changes in the Southern Hemisphere surface
824 westerlies. *Geophysical Research Letters* 48 (4): e2020GL090849. 2021.
825
826 Gremmen, N. J., B. Van De Vijver, Y. Frenot and M. Lebouvier. Distribution of moss-inhabiting diatoms along an altitudinal
827 gradient at sub-Antarctic Îles Kerguelen. *Antarctic Science* 19 (1): 17-24. 2007.
828
829 Humphries, R. S., M. D. Keywood, S. Gribben, I. M. McRobert, J. P. Ward, P. Selleck, S. Taylor, et al. Southern Ocean
830 latitudinal gradients of cloud condensation nuclei. *Atmos. Chem. Phys.* 21 (16): 12757-12782. doi: 10.5194/acp-21-12757-
831 2021. 2021.
832
833 Jones, J. M., S. T. Gille, H. Goosse, N. J. Abram, P. O. Canziani, D. J. Charman, K. R. Clem, et al. Assessing recent trends in
834 high-latitude Southern Hemisphere surface climate. *Nature Climate Change* 6 (10): 917-926. doi: 10.1038/nclimate3103. 2016.
835
836 Juggins, S. C2 User Guide. Software for ecological and palaeoecological data analysis and visualisation. Newcastle-uponTyne,
837 UK: University of Newcastle. 2003.
838
839 Juggins, S. Quantitative reconstructions in palaeolimnology: new paradigm or sick science? *Quaternary Science Reviews* 64:
840 20-32. 2013.
841
842 Keenan, H. M. Modern and fossil terrestrial and freshwater habitats on subantarctic Macquarie Island. Macquarie University
843 Thesis. doi: <https://doi.org/10.25949/24796983.v1>. 1995.
844
845 Kennedy, B. and Y. M. Buckley. Use of seasonal epilithic diatom assemblages to evaluate ecological status in Irish lakes.
846 *Ecological Indicators* 129: 107853. doi: <https://doi.org/10.1016/j.ecolind.2021.107853>. 2021.
847
848 Kong, Z., A. Prata, P. May, A. Purich, Y. Huang and S. Siems. Intensifying precipitation over the Southern Ocean challenges
849 reanalysis-based climate estimates—Insights from Macquarie Island’s 45-year record. *EGU sphere* 2025: 1-25. 2025.
850

851 Le Quéré, C., M. R. Raupach, J. G. Canadell, G. Marland, L. Bopp, P. Ciais, T. J. Conway, et al. Trends in the sources and
852 sinks of carbon dioxide. *Nature Geoscience* 2 (12): 831-836. doi: 10.1038/ngeo689. 2009.
853
854 le Roux, P. C. and M. A. McGeoch. Rapid range expansion and community reorganization in response to warming. *Global*
855 *Change Biology* 14 (12): 2950-2962. doi: <https://doi.org/10.1111/j.1365-2486.2008.01687.x>. 2008.
856
857 Lee, J. E. and S. L. Chown. Range expansion and increasing impact of the introduced wasp *Aphidius matricariae* Haliday on
858 sub-Antarctic Marion Island. *Biological Invasions* 18 (5): 1235-1246. doi: 10.1007/s10530-015-0967-3. 2016.
859
860 Liao, M., U. Herzsuh, Y. Wang, X. Liu, J. Ni and K. Li. Lake diatom response to climate change and sedimentary events on
861 the southeastern Tibetan Plateau during the last millennium. *Quaternary Science Reviews* 241: 106409. 2020.
862
863 Löffler, E. Macquarie Island: A wind-molded natural landscape in the subantarctic. *Polar Geography* 8 (4): 267-286. 1984.
864
865 Marchant, R., B. Kefford, J. Wasley, C. King, J. Doube and D. Nuggeoda. Response of stream invertebrate communities to
866 vegetation damage from overgrazing by exotic rabbits on subantarctic Macquarie Island. *Marine and freshwater research* 62
867 (4): 404-413. 2011.
868
869 Marshall, G. J. Trends in the Southern Annular Mode from observations and reanalyses. *Journal of climate* 16 (24): 4134-
870 4143. 2003.
871
872 Maslennikova, A. V. e. Development and application of an electrical conductivity transfer function, using diatoms from lakes
873 in the Urals, Russia. *Journal of Paleolimnology* 63 (2): 129-146. 2020.
874
875 McBride, T. Freshwater diatoms on sub-antarctic Macquarie Island: an ecological survey of 14 lakes. 2009.
876
877 McBride, T. P. and J. M. Selkirk. Palaeolake diatoms on sub-Antractic Macquarie Island: Possible markers of climate change.
878 *Data Symposium* 1998.
879
880 Menviel, L. C., P. Spence, A. E. Kiss, M. A. Chamberlain, H. Hayashida, M. H. England and D. Waugh. Enhanced Southern
881 Ocean CO₂ outgassing as a result of stronger and poleward shifted southern hemispheric westerlies. *Biogeosciences* 20 (21):
882 4413-4431. 2023.
883
884 Meredith, K., S. Hollins, C. Hughes, D. Cendón, S. Hankin and D. Stone. Temporal variation in stable isotopes (¹⁸O and ²H)
885 and major ion concentrations within the Darling River between Bourke and Wilcannia due to variable flows, saline
886 groundwater influx and evaporation. *Journal of Hydrology* 378 (3-4): 313-324. 2009.
887
888 Meredith, K. T., K. M. Saunders, L. K. McDonough and M. McGeoch. Hydrochemical and isotopic baselines for understanding
889 hydrological processes across Macquarie Island. *Scientific Reports* 12 (1): 21266. doi: 10.1038/s41598-022-25115-3. 2022.
890
891 Molén, M. O. Geochemical proxies: Paleoclimate or paleoenvironment? *Geosystems and Geoenvironment* 3 (1): 100238.
892 2024.
893
894 Mongwe, P., L. Gregor, J. Tjiputra, J. Hauck, T. Ito, C. Danek, M. Vichi, S. Thomalla and P. M. S. Monteiro. Projected
895 poleward migration of the Southern Ocean CO₂ sink region under high emissions. *Communications Earth & Environment* 5
896 (1): 232. doi: 10.1038/s43247-024-01382-y. 2024.
897
898 Nel, W., D. W. Hedding and E. M. Rudolph. The sub-Antarctic islands are increasingly warming in the 21st century. *Antarctic*
899 *Science* 35 (2): 124-126. 2023.
900

901 Nicholson, S.-A., D. B. Whitt, I. Fer, M. D. du Plessis, A. D. Lebéhot, S. Swart, A. J. Sutton and P. M. S. Monteiro. Storms
902 drive outgassing of CO₂ in the subpolar Southern Ocean. *Nature Communications* 13 (1): 158. doi: 10.1038/s41467-021-
903 27780-w. 2022.

904

905 Oksanen, J., F. G. Blanchet, R. Kindt, P. Legendre, P. R. Minchin, R. O'hara, G. L. Simpson, P. Solymos, M. H. H. Stevens
906 and H. Wagner. Package 'vegan'. *Community ecology package*, version 2 (9): 1-295. 2013.

907

908 Olivier, L. and F. A. Haumann. Southern Ocean freshening stalls deep ocean CO₂ release in a changing climate. *Nature Climate*
909 *Change* 15 (11): 1219-1225. doi: 10.1038/s41558-025-02446-3. 2025.

910

911 Peng, Y., P. Rioual and Z. Jin. A record of Holocene climate changes in central Asia derived from diatom-inferred water-level
912 variations in Lake Kalakuli (Eastern Pamirs, western China). *Frontiers in Earth Science* 10: 825573. 2022.

913

914 Perren, B. B., D. A. Hodgson, S. J. Roberts, L. Sime, W. Van Nieuwenhuyze, E. Verleyen and W. Vyverman. Southward
915 migration of the Southern Hemisphere westerly winds corresponds with warming climate over centennial timescales.
916 *Communications Earth and Environment* 1 (1). doi: 10.1038/s43247-020-00059-6. 2020.

917

918 Perren, B. B., J. Kaiser, H. W. Arz, O. Dellwig, D. A. Hodgson and F. Lamy. Poleward displacement of the Southern
919 Hemisphere Westerlies in response to Early Holocene warming. *Communications Earth & Environment* 6 (1): 164. doi:
920 10.1038/s43247-025-02129-z. 2025.

921

922 Recasens, C., D. Ariztegui, N. I. Maidana, B. Zolitschka and P. S. Team. Diatoms as indicators of hydrological and climatic
923 changes in Laguna Potrok Aike (Patagonia) since the Late Pleistocene. *Palaeogeography, Palaeoclimatology, Palaeoecology*
924 417: 309-319. 2015.

925

926 Roberts, D., A. McMinn and D. Zwartz. An initial palaeosalinity history of Jaw Lake, Bungler Hills based on a diatom–salinity
927 transfer function applied to sediment cores. *Antarctic Science* 12 (2): 172-176. 2000.

928

929 Sabbe, K., W. Vyverman, L. Ector, C. E. Wetzel, J. John, D. A. Hodgson, E. Verleyen and B. Van de Vijver. On the identity
930 of *Navicula gottlandica* (Bacillariophyta), with the description of two new species *Navicula eileencoxiana* and *Navicula*
931 *bergstromiana* from the Australo-Pacific region. *Plant Ecology and Evolution* 152 (2): 313-326. Accessed 2025/02/27/.
932 <https://www.jstor.org/stable/26672975>. 2019.

933

934 Saunders, K. M., J. J. Harrison, D. A. Hodgson, R. de Jong, F. Mauchle and A. McMinn. Ecosystem impacts of feral rabbits
935 on World Heritage sub-Antarctic Macquarie Island: A palaeoecological perspective. *Anthropocene* 3: 1-8. doi:
936 <https://doi.org/10.1016/j.ancene.2014.01.001>. 2013.

937

938 Saunders, K. M., D. A. Hodgson and A. McMinn. Quantitative relationships between benthic diatom assemblages and water
939 chemistry in Macquarie Island lakes and their potential for reconstructing past environmental changes. *Antarctic Science* 21
940 (1): 35-49. doi: 10.1017/S0954102008001442. 2009.

941

942 Saunders, K. M., D. A. Hodgson, S. McMurtrie and M. Grosjean. A diatom-conductivity transfer function for reconstructing
943 past changes in the Southern Hemisphere westerly winds over the Southern Ocean. *Journal of Quaternary Science* 30 (5): 464-
944 477. doi: 10.1002/jqs.2788. 2015.

945

946 Saunders, K. M., S. J. Roberts, B. Perren, C. Butz, L. Sime, S. Davies, W. Van Nieuwenhuyze, M. Grosjean and D. A. Hodgson.
947 Holocene dynamics of the Southern Hemisphere westerly winds and possible links to CO₂ outgassing. *Nature Geoscience* 11
948 (9): 650-655. doi: 10.1038/s41561-018-0186-5. 2018.

949

950 Scott, J. and J. Kirkpatrick. Rabbits, landslips and vegetation change on the coastal slopes of subantarctic Macquarie Island,
951 1980–2007: implications for management. *Polar Biology* 31 (4): 409-419. 2008.

952

953 Selkirk-Bell, J. and P. Selkirk. Vegetation-banked terraces on Subantarctic Macquarie Island: a reappraisal. *Arctic, antarctic,
954 and alpine research* 45 (2): 261-274. 2013.

955

956 Selkirk, P., R. Seppelt and D. Selkirk. *Subantarctic Macquarie Island: environment and biology*: Cambridge University Press.
957 1990.

958

959 Shaw, J., A. Terauds and D. Bergstrom. Rapid commencement of ecosystem recovery following aerial baiting on sub-Antarctic
960 Macquarie Island. *Ecological Management & Restoration* 12 (3): 241-244. 2011.

961

962 Springer, K. Eradication of invasive species on Macquarie Island to restore the natural ecosystem. *Recovering Australian
963 threatened species: A book of hope*: 13-22. 2018.

964

965 Sterken, M., E. Verleyen, V. Jones, D. Hodgson, W. Vyverman, K. Sabbe and B. Van de Vijver. An illustrated and annotated
966 checklist of freshwater diatoms (Bacillariophyta) from Livingston, Signy and Beak Island (Maritime Antarctic Region). *Plant
967 Ecology and Evolution* 148 (3): 431-455. 2015.

968

969 Sterken, M., E. Verleyen, K. Sabbe, G. Terry, F. Charlet, S. Bertrand, X. Boës, N. Fagel, M. De Batist and W. Vyverman.
970 Late Quaternary climatic changes in southern Chile, as recorded in a diatom sequence of Lago Puyehue (40° 40' S). *Journal of
971 Paleolimnology* 39 (2): 219-235. 2008.

972

973 ter Braak, C. J. and S. Juggins. Weighted averaging partial least squares regression (WA-PLS): an improved method for
974 reconstructing environmental variables from species assemblages. *Hydrobiologia* 269 (1): 485-502. 1993.

975

976 Ter Braak, C. J. and I. C. Prentice. A theory of gradient analysis. In *Advances in ecological research*, 271-317: Elsevier. 1988.

977

978 Terauds, A. Changes in rabbit numbers on Macquarie Island 1974–2008. Report to Tasmanian Parks and Wildlife Service.
979 2009.

980

981 Thomas, Z. A., H. Cadd, C. Turney, L. Becerra-Valdivia, H. A. Haines, C. Marjo, C. Fogwill, S. Carter and P. Brickle. Westerly
982 wind shifts drove Southern Hemisphere mid-latitude peat growth since the last glacial. *Nature Geoscience*. doi:
983 10.1038/s41561-025-01842-w. 2025.

984

985 Van de Vijver, B., Y. Freynot and L. Beyens. Freshwater diatoms from Ile de la Possession (Crozet archipelago, Subantarctica).
986 *Bibliotheca Diatomologica* 46: 1-412. 2002.

987

988 Van de Vijver, B. *Aulacoseira principissa* sp. nov., a new 'centric' diatom species from the sub-Antarctic region. *Phytotaxa* 52:
989 33–42. 2012.

990

991 Van de Vijver, B. Revision of the *Psammothidium manguinii* complex (Bacillariophyta) in the sub-Antarctic Region with the
992 description of four new taxa. *Fottea* 19 (1): 90-106. doi: 10.5507/fot.2019.001. 2019.

993

994 Van Nieuwenhuyze, W. 2020. Diatom species and limnological data from 64 lakes on subantarctic Marion Island (2011) [Data
995 set]. UK Polar Data Centre, Natural Environment Research Council, UK Research & Innovation.

996

997 Verleyen, E., D. A. Hodgson, K. Sabbe, K. Vanhoutte and W. Vyverman. Coastal oceanographic conditions in the Prydz Bay
998 region (East Antarctica) during the Holocene recorded in an isolation basin. *The Holocene* 14 (2): 246-257. 2004.

999

1000 Verleyen, E., D. A. Hodgson, W. Vyverman, D. Roberts, A. McMinn, K. Vanhoutte and K. Sabbe. Modelling diatom responses
1001 to climate induced fluctuations in the moisture balance in continental Antarctic lakes. *Journal of Paleolimnology* 30: 195-215.
1002 2003.
1003
1004 Volik, O., R. M. Petrone, R. I. Hall, M. L. Macrae, C. M. Wells, M. C. Elmes and J. S. Price. Long-term precipitation-driven
1005 salinity change in a saline, peat-forming wetland in the Athabasca Oil Sands Region, Canada: a diatom-based
1006 paleolimnological study. *Journal of Paleolimnology* 58 (4): 533-550. 2017.
1007
1008